Eur. Phys. J. C (2015) 75:29
DOI 10.1140/epjc/s10052-014-3243-2

THE EUROPEAN PHYSICAL JOURNAL C

Regular Article - Theoretical Physics

Squark production and decay matched with parton showers at NLO

R. Gavin[1,a], **C. Hangst**[2,b], **M. Krämer**[3,c], **M. Mühlleitner**[2,d], **M. Pellen**[3,e], **E. Popenda**[1,f], **M. Spira**[1,g]

[1] Paul Scherrer Institut, 5232 Villigen PSI, Switzerland
[2] Institute for Theoretical Physics, Karlsruhe Institute of Technology, 76128 Karlsruhe, Germany
[3] Institute for Theoretical Particle Physics and Cosmology, RWTH Aachen University, 52056 Aachen, Germany

Received: 26 August 2014 / Accepted: 22 December 2014 / Published online: 27 January 2015

Abstract Extending previous work on the predictions for the production of supersymmetric (SUSY) particles at the LHC, we present the fully differential calculation of the next-to-leading order (NLO) SUSY-QCD corrections to the production of squark and squark–antisquark pairs of the first two generations. The NLO cross sections are combined with the subsequent decay of the final state (anti)squarks into the lightest neutralino and (anti)quark at NLO SUSY-QCD. No assumptions on the squark masses are made, and the various subchannels are taken into account independently. In order to obtain realistic predictions for differential distributions the fixed-order calculations have to be combined with parton showers. Making use of the Powheg method we have implemented our results in the Powheg-Box framework and interfaced the NLO calculation with the parton shower Monte Carlo programs Pythia6 and Herwig++. The code is publicly available and can be downloaded from the Powheg-Box webpage. The impact of the NLO corrections on the differential distributions is studied and parton shower effects are investigated for different benchmark scenarios.

Contents

[a] e-mail: ryan.gavin@psi.ch
[b] e-mail: christian.hangst@kit.edu
[c] e-mail: mkraemer@physik.rwth-aachen.de
[d] e-mail: margarete.muehlleitner@kit.edu
[e] e-mail: pellen@physik.rwth-aachen.de
[f] e-mail: eva.popenda@psi.ch
[g] e-mail: michael.spira@psi.ch

1 Introduction

Among the numerous extensions of the standard model (SM), supersymmetric (SUSY) [1–11] constitutes one of the most attractive and most intensely studied options. SUSY allows to cure some of the flaws of the SM like the hierarchy problem or the existence of dark matter, for which SUSY with R-parity conservation provides a natural candidate. Thus one of the main tasks of the LHC is the search for SUSY particles. With the next run of the LHC at high energy it will be possible to search for the colour-charged SUSY particles, the squarks ($\tilde{q}$) and gluinos ($\tilde{g}$), in the multi-TeV mass range [12–14]. In R-parity conserving SUSY, they are copiously produced in pairs through the main SUSY-QCD production processes at the LHC, $pp \to \tilde{q}\tilde{q}, \tilde{q}\bar{\tilde{q}}, \tilde{q}\tilde{g}$ and $\tilde{g}\tilde{g}$.

The pair production cross sections for strongly-interacting SUSY particles have been provided at leading order (LO)

quite some time ago [15–18]. The next-to-leading order (NLO) SUSY-QCD corrections have been completed about ten years later in [19–22]. In these calculations the squark masses have been assumed to be degenerate, with the exception of stop pair production, where all squarks but the stop have been taken degenerate. The NLO corrections turned out to be large, increasing the cross sections by 5–90 % depending on the process and on the SUSY scenario under consideration. Furthermore, the inclusion of the NLO corrections reduces the uncertainties due to the unknown higher order corrections, reflected in the dependence of the cross section on the unphysical factorization and renormalization scales, from about ± 50 % at LO to ± 15 % at NLO. In view of the still large corrections at NLO, calculations have been performed beyond NLO, including resummation and threshold effects [23–37]. These corrections lead to a further increase by up to 10 % of the inclusive cross section and reduce the scale uncertainty further. Also electroweak contributions have been considered [38,39], and their NLO corrections, calculated in [40–46], have been shown to be significant, depending on the model and the flavour and chirality of the final state squarks.

The computation of the cross sections at LO and NLO SUSY-QCD can be performed with the publicly available computer program Prospino [47]. Based on the calculations in [21,22], the NLO corrections, however, are only evaluated for degenerate squark masses. Additionally, the loop-corrected cross sections for the various subchannels of the different flavour and chirality combinations are summed up. Though results for the individual subchannels can be obtained, they are provided in the approximation of scaling the exact LO cross section of the individual subchannel with a global K-factor, that is given by the ratio of the total NLO cross section and the total LO cross section for degenerate squark masses.[1] In this approximation it is assumed that the K-factors of the different subchannels do not vary significantly. In principal, the program also allows for the computation of the NLO differential distributions in the transverse momentum and the rapidity of the SUSY particles, based on the results in [21]. There it was found that the distributions for the investigated SUSY scenarios were only mildly distorted by the NLO corrections, and it has thus been assumed that differential K-factors are rather flat in general.

Recently, results have been presented for the NLO SUSY-QCD corrections to squark pair production without any simplifying assumptions on the SUSY particle spectrum [48,49], and including the subsequent NLO decays of the final state squarks into a quark and neutralino.[2] In [53] completely general NLO squark and gluino production cross sections based on the MADGOLEM framework have been provided and compared to resummed predictions from jet merging. In [54–56], we have calculated the NLO corrections to the pair production of squarks of the first two generations and implemented the cross section in a fully flexible partonic Monte Carlo program without making any simplifying assumptions on the squark masses and treating the different subchannels individually. In the course of this calculation we have developed a new gauge-independent approach for the subtraction of on-shell intermediate gluinos at the fully differential level and compared our approach to several methods proposed in the literature. Moreover, we have extended the results [48,49,53], by matching our NLO calculation to parton showers using the Powheg-Box [57–59] framework.

These recent NLO calculations which take into account the full mass spectrum have shown that the K-factors of the individual subchannels can vary by up to 20 %. Therefore, in order to improve the accuracy of the cross section predictions a proper NLO treatment of the individual subchannels is necessary, without relying on an averaged K-factor. Furthermore, it was found, that while the shapes of semi-inclusive distributions are only mildly affected by NLO corrections, this is not the case for more exclusive observables. Here the K-factors can vary by up to ± 20 % depending on the kinematics, both at the production level and after including squark decays supplemented by the clustering of partons to form jets. Irrespective of the use of fixed or dynamical scales, simply scaling LO distributions with a global K-factor is not a good approximation for exclusive observables.

In continuation of our effort to provide accurate predictions for SUSY production processes at the LHC we present in this work our results for the NLO SUSY-QCD corrections to squark–antisquark production of the first two generations. We furthermore combine our results both for squark pair production and for squark–antisquark production with the decay of the (anti)squark into the lightest neutralino and (anti)quark at NLO SUSY-QCD. All results are obtained at fully exclusive level and without making any simplifying assumptions on the squark mass spectrum. In order to obtain realistic predictions for exclusive observables we have combined our fixed-order NLO calculations with parton showers. To this end, the processes have been implemented in the Powheg-Box framework [56,59] and interfaced with different parton shower programs. The implementation has been made publicly available and can be obtained from [60].

[1] Note that this is only possible with the second version of Prospino, called Prospino2. Although the original version could be modified to return also results for the separate channels, in its public version it returns all LO and NLO subchannels summed up.

[2] A complete NLO study of top-squark pair production at the LHC, including QCD and EW corrections has been published in [50]. In [51,52] NLO SUSY-QCD effects have been taken into account for top-squark pair production and decay.

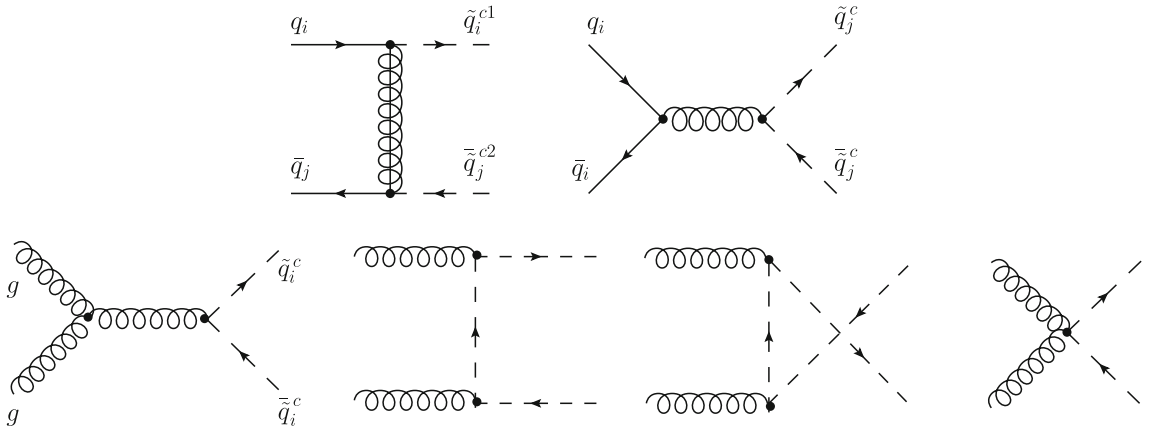

Fig. 1 Feynman diagrams contributing to squark–antisquark production at LO

The outline of the paper is as follows. In Sect. 2 we present the NLO calculation of the squark–antisquark production process. Section 3 is devoted to the computation of the squark decays at NLO and the combination with the production processes. Here we study different approaches for the consistent combination at NLO. The implementation in the Powheg-Box as well as our results at fixed order and including parton shower effects are presented in Sect. 4. Finally, we compare our results with results obtained with an approximate approach used in the SUSY searches by the LHC experiments. We summarize and conclude in Sect. 5.

2 Squark–antisquark production at NLO

The calculation of the NLO corrections to squark–antisquark production is very similar to the one for squark pair production already presented in [54]. Therefore, the following discussion summarizes only the main steps and points out the most important differences between the two processes.

2.1 Contributing channels

The production of a squark–antisquark pair at LO either proceeds via a pair of gluons or a quark-antiquark pair in the initial state:

$$\begin{aligned} q_i\,\bar{q}_j &\to \tilde{q}_k^{c1}\,\bar{\tilde{q}}_l^{c2}, \\ g\,g &\to \tilde{q}_i^{c}\,\bar{\tilde{q}}_i^{c}. \end{aligned} \tag{1}$$

Here, the lower indices indicate the flavour of the particle, whereas the upper indices for the squarks denote the respective chirality. The contributing Feynman diagrams are depicted in Fig. 1. Due to the flavour conserving structure of the occurring vertices the gg initiated diagrams and the s-channel diagram contribute only to the production of squarks of the same flavour and chirality. The results for the individual matrix elements squared can be found in [56].

We consider in the following only the production of squarks of the first two generations mediated by the strong interaction. Correspondingly, the higher-order calculation comprises only SUSY-QCD corrections. In total, this leads to 64 possible final state combinations. This number can be reduced to 36 independent channels if the invariance under charge conjugation is taken into account. The number of independent channels can be reduced further if some of the squark masses are degenerate, as in this case the results for the $q\bar{q}$ initiated contributions differ only in the respective PDFs. However, we perform the calculation for a general mass spectrum and take advantage of this point only in the numerical analysis.

2.2 Virtual and real corrections

At NLO the squark–antisquark production processes receive contributions from virtual and real corrections. For the calculation of the virtual corrections we use the Mathematica packages FeynArts 3.8 [61–63] and FormCalc 6.1 [64,65]. The numerical evaluation of the loop integrals is performed with Looptools 2.7 [64,66].

In order to regularise the occurring ultraviolet (UV) divergences we apply dimensional regularisation (DR) [67–71]. The UV divergences are absorbed into the fields and parameters of the theory by introducing renormalization constants. For the renormalization of the strong coupling constant we use the $\overline{\text{MS}}$ scheme and decouple the heavy particles, i.e. the gluino, the top-quark and the squarks, from the running of the strong coupling constant α_s. In the numerical analysis the 2-loop results for the determination of α_s at the scale of the process are used, hence we require the 1-loop decoupling coefficient, which can be found e.g. in [21,72–74]. Dimensional regularisation violates SUSY explicitly by changing the number of df of the gluon field, inducing a mismatch between the gauge and the Yukawa couplings beyond LO. At NLO this effect can be cured by adding a finite SUSY restor-

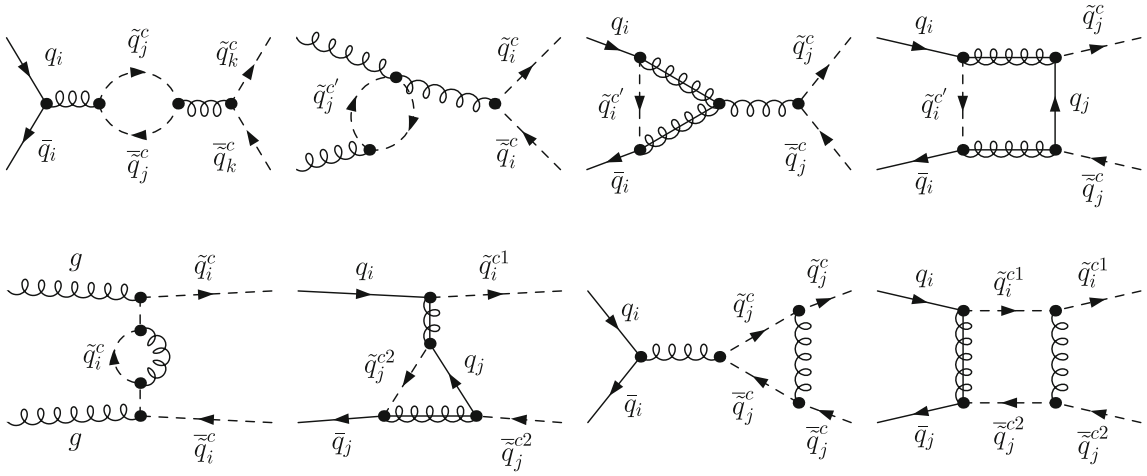

Fig. 2 Sample Feynman diagrams contributing to the virtual corrections of squark–antisquark production

ing counterterm to the counterterm of the Yukawa coupling, see [75]. With these steps it is possible to use the five-flavour $\alpha_s^{(5),\overline{\text{MS}}}$ in the numerical analysis. The occurring fields and masses are renormalized using on-shell renormalization conditions. As the relevant counterterms are not included in the FormCalc version we use, they had to be implemented by hand in the MSSM model file.

The actual calculation of the corrections is performed such that the full mass dependence is preserved. In principle this requires the generation of all possible production modes with FeynArts, which is obviously a very inefficient procedure. Instead, we generated only the virtual contributions for $u\bar{u} \to \tilde{u}_L\bar{\tilde{u}}_L$, $u\bar{u} \to \tilde{u}_L\bar{\tilde{u}}_R$, $u\bar{d} \to \tilde{u}_L\bar{\tilde{d}}_L$, $d\bar{d} \to \tilde{u}_L\bar{\tilde{u}}_L$ and $gg \to \tilde{u}_L\bar{\tilde{u}}_L$, where the indices L and R refer to the left- and right-handed chirality of the squarks. All other combinations of squarks in the final state can be traced back to one of these cases. However, this procedure requires a generalization of the masses of the internal squarks, if the corresponding propagators are connected to an external squark or quark line. In case of squark pair production this step amounted to simply replacing all internal squark masses in the vertex and box corrections with the masses of the external squarks, while the self-energy corrections could be left unchanged. For squark–antisquark production this generalization is more involved and requires a dedicated consideration of the individual diagrams. Some sample graphs are depicted in Fig. 2. The first two diagrams in the upper row are examples for the case where all internal masses have to be kept, i.e. here no changes are necessary. In the next two graphs the masses of the squarks in the loop have to be replaced case by case according to the flavour of the initial state quarks. Note that both chiralities have to be taken into account. The diagrams depicted in the lower row of the figure are examples for the case where one or more internal squarks are connected directly or indirectly to the final state squarks. The masses in the corresponding propagators and loop integrals have to be generalized accordingly.

The real corrections consist of the contributions with one additional gluon in the final state:

$$\begin{aligned} q_i\,\bar{q}_j &\to \tilde{q}_k^{c1}\,\bar{\tilde{q}}_l^{c2}\,g, \\ g\,g &\to \tilde{q}_i^{c}\,\bar{\tilde{q}}_i^{c}\,g. \end{aligned} \tag{2}$$

Moreover, at NLO a new channel occurs with a gluon and an (anti)quark in the initial state:

$$\begin{aligned} q_i\,g &\to \tilde{q}_k^{c1}\,\bar{\tilde{q}}_l^{c2} q_j, \\ g\,\bar{q}_j &\to \tilde{q}_k^{c1}\,\bar{\tilde{q}}_l^{c2} \bar{q}_i. \end{aligned} \tag{3}$$

These channels are related to each other by invariance under charge conjugation.

In order to calculate the $q_i\bar{q}_j$, $q_i g$ and $g\bar{q}_j$ channels it is sufficient to perform the calculation for one of them and construct the other combinations by either crossing the gluon or by charge conjugating the respective process. Here, the calculation is performed analytically for the $q_i g \to \tilde{q}_k^{c1}\,\bar{\tilde{q}}_l^{c2} q_j$ subprocesses. The occurring traces are evaluated with FeynCalc 8.2 [76]. The calculation is performed using two gauges for the external gluon, the Feynman gauge and a light-cone gauge.

The gg-channels are obtained from MadGraph 5.1.3.1 [77] by generating the HELAS calls [78] for the specific process $gg \to \tilde{u}_L\,\bar{\tilde{u}}_L g$, generalizing the masses of the occurring squarks and removing the widths of the intermediate particles.

All these contributions exhibit infrared (IR) divergences, which cancel by virtue of the Kinoshita–Lee–Nauenberg theorem [79,80] against the corresponding divergences in the virtual contributions. As apt for a Monte Carlo event generator this cancellation is achieved by means of a subtraction formalism. We employ the FKS method [81], which is automated in the Powheg-Box.

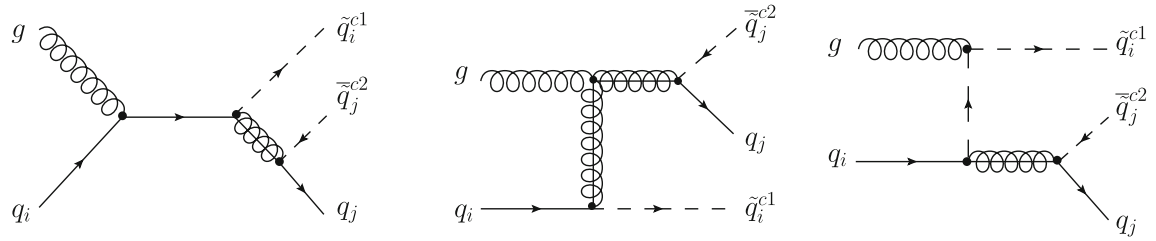

Fig. 3 Feynman diagrams contributing to the real corrections of squark–antisquark production with potentially on-shell intermediate gluinos

In the qg-initiated channels $q_i g \to \tilde{q}_i \bar{\tilde{q}}_j q_j$ a second type of singularity occurs for scenarios with $m_{\tilde{g}} > m_{\tilde{q}_j}$.[3] For these mass configurations the intermediate gluino in the diagrams depicted in Fig. 3 can be produced on-shell, causing a resonant behaviour. A similar problem has already been encountered in the calculation of squark pair production [21,54]. Being formally equivalent to the Born contribution of on-shell squark–gluino production with the gluino decaying subsequently into a quark and an antisquark these contributions are large and require a proper definition of the process of interest. Keeping these terms would cause a double counting if the predictions for squark–antisquark production were combined with the ones for squark–gluino production. A fully inclusive treatment of coloured SUSY particle production would be free of these ambiguities but the treatment of resonant intermediate states still requires a consistent method to introduce finite width effects. This can be achieved by e.g. the complex-mass scheme [82] or the method that has been introduced in [54] and will be described in the following. However, since the fully inclusive calculation is not yet available and beyond the scope of our work, meaningful results for individual production processes can only be obtained with the on-shell contributions subtracted consistently.

There exist several methods to cope with this type of singularities, which have been developed in the context of tW production [83], squark pair production [48,54] and squark/gluino production [21]. These approaches can be categorized as follows:

- *Diagram removal* (*DR*) In this approach the resonant contributions are removed by either completely neglecting the Feynman diagrams in Fig. 3 (DR-I) or by keeping the interference terms with the non-resonant contributions, but removing the amplitude squared of the depicted graphs (DR-II). Both approaches are rather easy to implement in a Monte Carlo program, but break gauge invariance.

[3] An equivalent problem appears in the $\bar{q}_i g \to \bar{q}_j \bar{\tilde{q}}_i \bar{q}_j$ channels. However, these contributions are related to the $q_i g$ case by charge conjugation and have been treated accordingly. They will not be discussed explicitly in the following.

- *Diagram subtraction* (*DS*) These methods aim at a pointwise subtraction of the on-shell contributions by constructing a counterterm and performing a suitable reshuffling of the momenta. Hence both the interference terms and the off-shell contributions are kept by construction. In order to regularise the singular behaviour for $(p_{\tilde{q}_j} + p_{q_j})^2 \to m_{\tilde{g}}^2$ a finite width $\Gamma_{\tilde{g}}$ for the resonant gluino has to be introduced (in fact this is also required in the DR-II scheme in order to regularise the integrable singularity in the interference terms). In the original proposal for tW production [83] this is achieved by replacing the corresponding propagator:

$$\frac{1}{(p_{\tilde{q}_j} + p_{q_j})^2 - m_{\tilde{g}}^2} \to \frac{1}{(p_{\tilde{q}_j} + p_{q_j})^2 - m_{\tilde{g}}^2 + i m_{\tilde{g}} \Gamma_{\tilde{g}}}. \tag{4}$$

However, this approach is only gauge invariant in the limit $\Gamma_{\tilde{g}} \to 0$. A fully gauge invariant modification of the DS scheme (denoted DS* in the following) has been proposed in the context of squark pair production [54]. In this approach the analytic expression for the amplitude squared is expanded in the poles $(p_{\tilde{q}_j} + p_{q_j})^2 - m_{\tilde{g}}^2 \equiv s_{jg}$ before introducing the regularising width:

$$|M_{\text{tot}}|^2 = \frac{f_0}{s_{jg}^2} + \frac{f_1}{s_{jg}} + f_2(s_{jg}). \tag{5}$$

The coefficients f_k $(k = 0, 1, 2)$ are gauge invariant quantities, i.e. introducing a regulator $\Gamma_{\tilde{g}}$ at this point preserves gauge invariance and leads to

$$|M_{\text{tot}}|^2 = \frac{f_0}{s_{jg}^2 + m_{\tilde{g}}^2 \Gamma_{\tilde{g}}^2} + \frac{s_{jg}}{s_{jg}^2 + m_{\tilde{g}}^2 \Gamma_{\tilde{g}}^2} f_1 + f_2(s_{jg}). \tag{6}$$

The differences between the expressions obtained with the DS* and with the 'usual' DS method vanish for $\Gamma_{\tilde{g}} \to 0$ as expected, see [54]. The counterterm for the subtraction of the on-shell contributions in this method is given by f_0 and reproduces the one used in the DS scheme in the limit $(p_{\tilde{q}_j} + p_{q_j})^2 \to m_{\tilde{g}}^2$. For more details

Table 1 The NLO cross sections for squark–antisquark production of the first generation obtained for the CMSSM point 10.4.5 applying the DS* scheme (second column) and the DR-II method (third column), with $\Delta_\sigma \equiv \left(\sigma^{\text{DS}^*} - \sigma^{\text{DR-II}}\right)/\sigma^{\text{DS}^*}$. The charge conjugate channels are combined. The last four columns contain the numerical values for the quantity σ_{qg} as defined in the text and the respective contribution to the full NLO cross section, again for both the DS* and the DR-II method

Process	σ^{DS^*} (fb)	$\sigma^{\text{DR-II}}$ (fb)	Δ_σ (%)	$\sigma_{qg}^{\text{DS}^*}$ (fb)	$\frac{\sigma_{qg}^{\text{DS}^*}}{\sigma^{\text{DS}^*}}$ (%)	$\sigma_{qg}^{\text{DR-II}}$ (fb)	$\frac{\sigma_{qg}^{\text{DR-II}}}{\sigma^{\text{DR-II}}}$ (%)
$\tilde{u}_L\bar{\tilde{u}}_L$	1.74×10^{-1}	1.67×10^{-1}	4.09	1.60×10^{-3}	0.92	-5.46×10^{-3}	−3.27
$\tilde{u}_R\bar{\tilde{u}}_R$	2.31×10^{-1}	2.24×10^{-1}	3.06	-5.71×10^{-4}	−0.25	-7.56×10^{-3}	−3.38
$\tilde{d}_L\bar{\tilde{d}}_L$	1.15×10^{-1}	1.13×10^{-1}	2.02	-3.38×10^{-3}	−2.94	-5.67×10^{-3}	−5.03
$\tilde{d}_R\bar{\tilde{d}}_R$	1.64×10^{-1}	1.62×10^{-1}	1.37	-6.02×10^{-3}	−3.66	-8.25×10^{-3}	−5.09
$\tilde{u}_L\bar{\tilde{u}}_R$	6.94×10^{-1}	6.79×10^{-1}	2.12	-9.44×10^{-3}	−1.36	-2.40×10^{-2}	−3.54
$\tilde{d}_L\bar{\tilde{d}}_R$	2.41×10^{-1}	2.36×10^{-1}	1.91	-3.41×10^{-3}	−1.42	-8.15×10^{-3}	−3.45
$\tilde{u}_L\bar{\tilde{d}}_L$	8.42×10^{-2}	7.49×10^{-2}	11.1	7.80×10^{-3}	9.27	-1.55×10^{-3}	−2.07
$\tilde{u}_L\bar{\tilde{d}}_R$	4.92×10^{-1}	4.83×10^{-1}	1.88	-6.90×10^{-3}	−1.4	-1.60×10^{-2}	−3.3
$\tilde{u}_R\bar{\tilde{d}}_L$	4.84×10^{-1}	4.74×10^{-1}	2.09	-6.03×10^{-3}	−1.25	-1.63×10^{-2}	−3.44
$\tilde{u}_R\bar{\tilde{d}}_R$	1.09×10^{-1}	1.00×10^{-1}	8.33	7.47×10^{-3}	6.83	-1.64×10^{-3}	−1.64
Sum	2.79	2.71	2.72	−0.0189	−0.677	−0.0946	−3.49

on the momentum reshuffling and the construction of the subtraction term see [54].

The comparison of these different subtraction methods for squark pair production revealed for the scenario considered in [54] only discrepancies in the total cross section at the per mille level. Repeating this study for squark–antisquark production, however, leads to larger differences, as the contributions of the qg initiated channels are larger in this case. To illustrate this point the predictions for the total production cross sections of squarks of the first generation as obtained with the DR-II (using the light-cone gauge) and the DS* scheme are summarized in the second and third column of Table 1. The scenario considered here corresponds to the mSUGRA point 10.4.5 [84] specified in Sect. 4. For the regularising width we choose $\Gamma_{\tilde{g}} = 1\,\text{GeV}$. As can be inferred from the percental difference between the respective numbers given in the fourth column the predictions obtained with these two methods differ by up to 11 %, leading to a discrepancy of 2.7 % after summing these channels. Taking into account the contributions of the squarks of the second generation, too, increases this discrepancy further:

$$\sigma^{\text{DS}^*} = 4.37\,\text{fb} \quad \text{and} \quad \sigma^{\text{DR-II}} = 4.21\,\text{fb}, \tag{7}$$

corresponding to a discrepancy of 3.6 %.

The fifth and seventh column of Table 1 contain the respective predictions σ_{qg} for the qg contribution to each channel. This (unphysical) quantity comprises the $2 \to 3$ parts of the respective channel, i.e. the real amplitudes squared and the corresponding FKS counterterm and hence allows for a direct estimation of the effects of the applied subtraction scheme. As can be inferred from the table these contributions make up several percent of the individual cross sections. Hence the large discrepancies observed between the two subtraction methods have significant effects on the predictions for the total cross sections.

Even larger effects of the chosen subtraction scheme can be observed in differential distributions which are sensitive to the emitted parton of the real corrections. As an example, the p_T distribution of the radiated parton obtained with the DR-II scheme and the DS* method is shown in Fig. 4 (left). For $p_T^j > 200\,\text{GeV}$ the two predictions differ by about 30 %. In contrast, the shape of the $m^{\tilde{q}\bar{q}}$ distribution (right plot in Fig. 4), which is supposed to be less sensitive to additional radiation, is not affected by the chosen method. Solely the normalization reflects the 3.6 % discrepancy already encountered in the total cross section.

2.3 Tests and comparison

The calculation presented in the last section has undergone numerous checks and comparisons. An obvious test for the correctness of the calculation consists in a comparison with the public program Prospino2 for the limit of a mass degenerate spectrum. Unfortunately, a direct comparison of the results obtained with this public code is not straightforward, as it implicitly takes into account the sbottom production processes $gg \to \tilde{b}\bar{\tilde{b}}$ and $q\bar{q} \to \tilde{b}\bar{\tilde{b}}$, while the contributions $b\bar{b} \to \tilde{b}\bar{\tilde{b}}$ are neglected. Moreover, at NLO the contributions $qg \to \tilde{q}\bar{\tilde{b}}b$ and the charge conjugate processes are taken into account. Instead of mimicking the way the total K-factor is calculated in Prospino2 we have compared the numerical results of our calculation with a non-public implementation

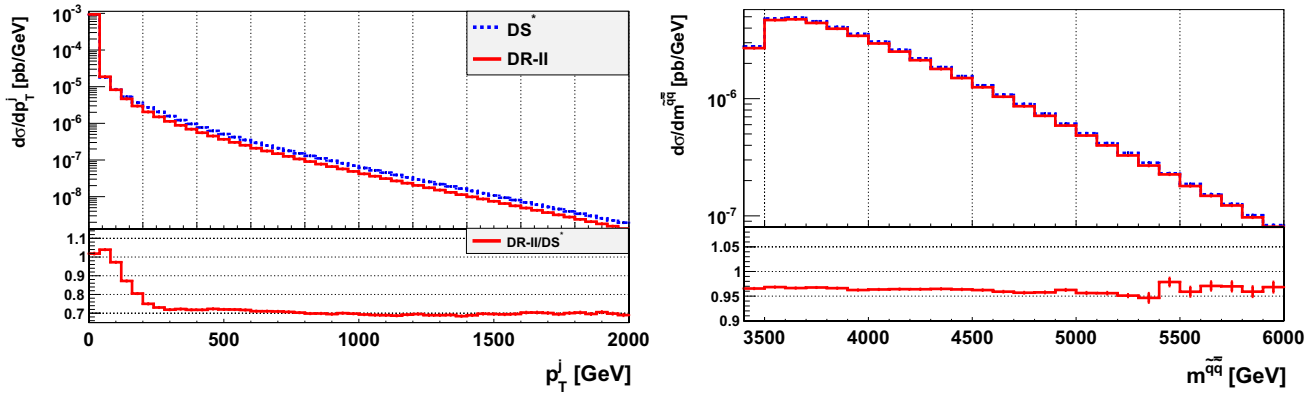

Fig. 4 The distributions for squark–antisquark production of the transverse momentum of the radiated parton generated in the real contributions, p_T^j, (*left*) and the invariant mass $m^{\tilde{q}\bar{\tilde{q}}}$ (*right*) for the subtraction methods DS* and DR-II. The *lower panels* show the respective ratio of the DR-II and the DS* result

of the original results from [21], denoted Prospino* in the following. Besides testing our calculation for the special case of degenerate squarks we have intensively checked the individual building blocks:

- The Born expressions have been compared with results given in the literature [16–18]. In addition, the numerical comparison of the total cross section with Prospino* provides a simple cross check for the correctness of the nontrivial combinatorics of the contributing channels.
- The UV finiteness of the virtual corrections has been checked both analytically and numerically. The correct structure of the IR poles has been verified by comparison with the known structure for the case of massive coloured particles in the final state, see e.g. [85]. The correctness of the modifications performed in the virtual routines in order to generalize them to an arbitrary mass spectrum has been tested by performing this generalization for both $gg \to \tilde{u}_L\bar{\tilde{u}}_L$ and $gg \to \tilde{d}_L\bar{\tilde{d}}_L$ and comparing the outcome numerically. Likewise, the other cases mentioned in Sect. 2.2 have been checked.
- The analytic results for the real matrix elements squared have been compared numerically for a multitude of arbitrary phase space points with the routines generated with MadGraph 5. The cancellation of the IR poles against the FKS counterterms has been tested using the automatic procedure provided by the Powheg-Box. The gauge invariance of the DS* scheme has been explicitly checked by comparing the outcome of the two different gauges used in the calculation. Furthermore, the equivalence of the DS and the DS* scheme in the limit $\Gamma_{\tilde{g}} \to 0$ has been verified numerically.
- The individual results for the three production channels gg, $q\bar{q}$ and qg have been compared for degenerate mass spectra with Prospino*.

3 Squark decays at NLO and combination with production processes

The calculation of NLO SUSY-QCD corrections to production processes is only a first step towards a realistic prediction of possible events at the LHC. The next step requires the inclusion of the decays of the produced particles. Here, only the decay mode into a quark and the lightest neutralino for squarks, $\tilde{q} \to q\tilde{\chi}_1^0$, or into an antiquark and the lightest neutralino for antisquarks, $\bar{\tilde{q}} \to \bar{q} + \tilde{\chi}_1^0$, will be taken into account. In many SUSY scenarios, in particular the ones studied in this paper, the lightest neutralino is the lightest supersymmetric particle and stable (if R-parity conservation is assumed). The SUSY-QCD corrections to this decay have been known for several years. However, in the original calculation [86] only results for the partial width have been given, so that a differential description is not possible. Recently, a fully differential calculation in the context of squark pair production and decay has been presented [48] where the radiative corrections to the decay have been included by using the phase-space-slicing technique. In the next subsection we present a recalculation of the decay at the fully differential level by applying the subtraction method developed for single top production and decay [87] to our process. The second part of this section deals with the consistent calculation of the total squark width, which is required for the combination of the production and decay processes described in the last part of this section.

3.1 Decay width for $\tilde{q} \to q + \tilde{\chi}_1^0$ at NLO

The LO contribution to the decay width of the process

$$\tilde{q} \to q + \tilde{\chi}_1^0 \tag{8}$$

comprises only one Feynman diagram, which is depicted in Fig. 5a. As in the production process, at NLO virtual and real

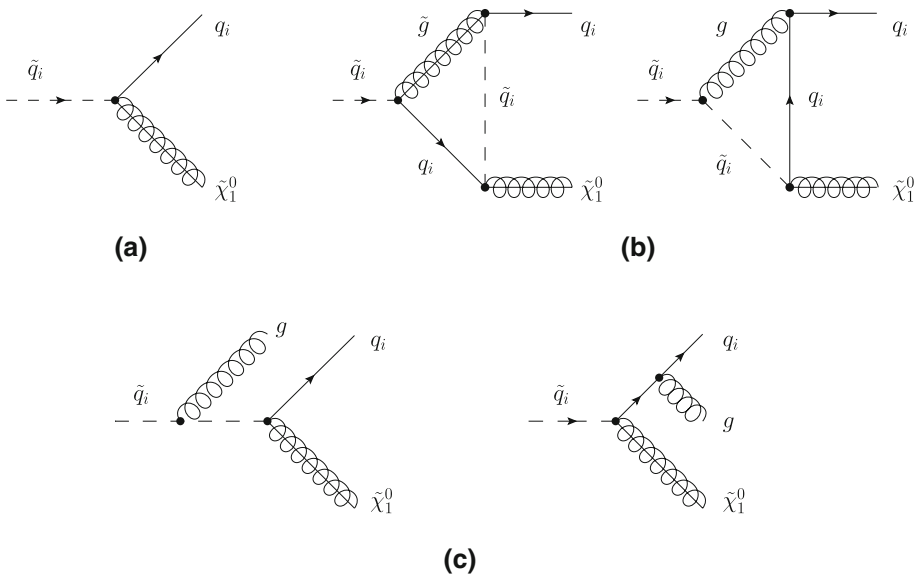

Fig. 5 Feynman diagrams contributing to the decay $\tilde{q}_i \to q_i \tilde{\chi}_1^0$ at LO (**a**) and at NLO: virtual corrections (**b**) and real gluon radiation (**c**)

corrections have to be taken into account. The two diagrams contributing to the virtual corrections are shown in Fig. 5b. The calculation is performed in DR and the external fields are renormalized on-shell. All integrals have been evaluated analytically. The package HypExp [88,89] has been used to expand hypergeometric functions. Using DR requires, again, the introduction of a finite counterterm. Here, the squark-quark-neutralino Yukawa coupling $\hat{g}$ is affected. The SUSY-restoring counterterm leads to the following relation to the gauge coupling g [75],

$$\hat{g} = g\left[1 - \frac{\alpha_s}{6\pi}\right]. \tag{9}$$

The real corrections involve an additional gluon,

$$\tilde{q} \to q + \tilde{\chi}_1^0 + g, \tag{10}$$

emitted either from the squark in the initial state or the quark in the final state, as displayed in Fig. 5c. The IR divergences arising from the soft and/or collinear emission of the gluon cancel against the corresponding ones in the virtual corrections. This cancellation is achieved on the differential level by applying the subtraction method developed in [87] for single top production and decay to our decay process. The divergences in the real radiation process are cancelled by a local counterterm, which is constructed such that it has the same singular behaviour as the full matrix element. It takes the form of the LO matrix element squared multiplied by a function D, which describes the emission of the soft or collinear radiation:

$$\left|\mathcal{M}_r\left(p_{\tilde{q}_i}, p_q, p_{\tilde{\chi}_1^0}, p_g\right)\right|^2 \to \left|\mathcal{M}_0\left(p_{\tilde{q}_i}, p'_q, p'_{\tilde{\chi}_1^0}\right)\right|^2 \times D\left(p_g \cdot p_{\tilde{q}_i}, p_g \cdot p_q, m^2_{\tilde{q}_i}, m^2_{\tilde{\chi}_1^0}\right). \tag{11}$$

In the limit of soft emission, when $p_g \to 0$, or where the momenta of the quark p_q and the gluon p_g are collinear, the counterterm on the right-hand side of Eq. (11) has the same singular structure as the full matrix element squared on the left-hand side. The LO matrix element $\mathcal{M}_0$ is evaluated with modified momenta p'_q and $p'_{\tilde{\chi}_1^0}$ which absorb the momentum carried away by the gluon. They are subject to momentum conservation $p_{\tilde{q}_i} = p'_q + p'_{\tilde{\chi}_1^0}$, as well as to the on-shell conditions $p'^2_q = 0$ and $p'^2_{\tilde{\chi}_1^0} = m^2_{\tilde{\chi}_1^0}$.

In the process at hand advantage can be taken from the fact that the LO matrix element squared can be easily factorized from the divergent part of the real matrix element squared,

$$\left|\mathcal{M}_r^{\mathrm{Div}}\right|^2 = \frac{4}{3}\frac{16\pi}{m^2_{\tilde{q}_i}}\,\alpha_s\,|\mathcal{M}_0|^2 f(y,z), \tag{12}$$

with the function $f(y,z)$, calculated in $d = 4 - 2\epsilon$ dimensions, defined as

$$f(y,z) = -\frac{1}{2}\frac{1}{(1-\sqrt{r})^2}\left(\frac{1+z}{y} + \frac{1-z}{y}\,\epsilon\right) + \frac{1}{(1-\sqrt{r})^2}\frac{1}{y(1-z)} - \frac{1}{(1-r)^2(1-z)^2}. \tag{13}$$

In this function the following substitutions have been made

$$p_q \cdot p_g = \frac{{m_{\tilde{q}_i}}^2}{2}(1-\sqrt{r})^2 y \quad \text{and}$$
$$p_{\tilde{q}} \cdot p_g = \frac{{m_{\tilde{q}_i}}^2}{2}(1-r)(1-z), \tag{14}$$

with r denoting the squared ratio of the neutralino over the squark mass,

$$r = m^2_{\tilde{\chi}^0_1}/m^2_{\tilde{q}_i}. \quad (15)$$

The coefficient of the LO matrix element squared in Eq. (12) can then be chosen to serve as the divergent part denoted by D in the counterterm in Eq. (11),

$$D\left(p_g \cdot p_{\tilde{q}_i}, p_g \cdot p_q, m^2_{\tilde{q}_i}, m^2_{\tilde{\chi}^0_1}\right) = \frac{4}{3}\frac{16\pi}{m^2_{\tilde{q}_i}}\,\alpha_s\, f(y,z). \quad (16)$$

In order to cancel the IR divergences in the virtual corrections this counterterm needs to be integrated analytically over the one-particle phase space of the emitted gluon. The results for the necessary integrals can be found in Table 1 of [87]. The integrated counterterm then reads

$$\int \mathrm{d}\Phi_1 \left|\mathcal{M}_r^{\mathrm{Div}}\right|^2 = \frac{4}{3}\frac{\alpha_s}{\pi}\left(\frac{4\pi}{m^2_{\tilde{q}_i}}\right)^{\epsilon} |\mathcal{M}_0|^2 \times \langle f(y,z)(1-\sqrt{r})^2\rangle, \quad (17)$$

with

$$\begin{aligned}\langle f(y,z)(1-\sqrt{r})^2\rangle &= \frac{1}{2\epsilon^2} + \frac{5}{4\epsilon} - \frac{1}{\epsilon}\ln(1-r) - \frac{5}{2}\ln(1-r) \\ &+ \frac{(7-5r)}{8(1-r)} - \mathrm{Li}_2(r) - \frac{7\pi^2}{24} - \frac{3}{2}\frac{r}{1-r}\ln r \\ &+ \frac{1}{4}\frac{r^2}{(1-r)^2}\ln r - \ln(r)\ln(1-r) + \ln^2(1-r) + \frac{11}{4}. \quad (18)\end{aligned}$$

All steps of the analytical calculation have been checked against [90]. The results for the partial widths at LO and NLO have been compared to the result obtained from Sdecay 1.3 [91]. Moreover, we have compared our results to the results presented in the independent calculation of squark pair production and decay of [48], in particular to the results given in Table 6 for the benchmark point 10.1.5 and the corresponding distributions, and have found agreement. In addition, this decay has been implemented in the Powheg-Box. The virtual corrections for this independent calculation have been calculated with FeynArts/FormCalc and the loop integrals have been evaluated with LoopTools. The real matrix elements squared, calculated by hand, have been tested numerically for a multitude of phase space points against the corresponding routines obtained with MadGraph. In the Powheg-Box the cancellation of the divergences is achieved automatically via the implemented FKS subtraction method. We have found perfect agreement between the calculation presented in this section and the implementation in the Powheg-Box.

3.2 Total squark width at NLO

For the calculation of the squark branching ratios we also need the total decay width $\Gamma^{\tilde{q}}_{\mathrm{tot}}$, both at LO and NLO. Furthermore, the NLO total decay width will be necessary to normalize the expressions for the combination of the production and decay processes, as we will see in the next subsection. Since we only consider the decay into a quark and the lightest neutralino as possible 'decay chain' for the produced squarks, it is not necessary to describe all other partial decay widths differentially. Therefore, they can be extracted from the literature or their implementation in Sdecay. In order to implement the various decay routines from Sdecay in our code the following adaptions had to be made for the individual decay modes:

- Electroweak decays: $\tilde{q}_i \to q_i \tilde{\chi}^0_k$ $(k = 1,2,3,4)$ and $\tilde{q}_i \to q_j \tilde{\chi}^{\pm}_l$ $(l = 1,2)$.
  The decays into neutralinos $\tilde{\chi}^0_k$ or charginos $\tilde{\chi}^{\pm}_l$ are mediated by electroweak interactions. The decay into charginos is only possible for left-chiral squarks. In the routines for the (N)LO results [86] taken from Sdecay only the conventions for the parameters, especially those entering the calculation of the squark-quark-gaugino vertex, had to be adapted. In our calculation the weak mixing angle θ_W is determined according to Eq. (10.11) from [92], yielding
  $$\sin^2\theta_W = \frac{1}{2} - \sqrt{\frac{1}{4} - \frac{\pi\alpha(m_Z)}{\sqrt{2}G_F m_Z^2}}. \quad (19)$$
  All other parameters needed for the numerical evaluation of the decay widths can be found in Sect. 4.2.
- Strong decay: $\tilde{q}_i \to q_i \tilde{g}$.
  The NLO corrections to this strong decay mode have been calculated in [93]. However, this calculation has been performed for degenerate squark masses and implemented in the same way in Sdecay. In order to incorporate the full mass dependence, we have calculated the gluino self energy using the corresponding function from the calculation of the stop decays [94]. In these decays the correct $\tilde{t}_{1,2}$ masses, the top quark mass and the $\tilde{t}$ mixing angles have been used. For each squark of the first two generations this function is called by replacing the appropriate squark mass and setting the quark mass and mixing angles to zero.
  Also in the calculation of α_s, where the heavy particles are decoupled from the running, the squark masses are assumed to be degenerate. To restore the full mass dependence in α_s, the logarithms of the masses of the heavy, decoupled particles have been modified to obtain the logarithms given in Eq. (3) of [54]. In Sdecay the strong coupling constant is converted from the $\overline{\mathrm{MS}}$ scheme, used in the original calculation, to the $\overline{\mathrm{DR}}$ scheme. In order to use α_s as implemented in the Powheg-Box we calculate α_s in the $\overline{\mathrm{MS}}$ scheme by omitting the conversion factor introduced in Sdecay.

3.3 Combination with the production processes

A consistent combination of the production processes at NLO with the subsequent decays of the squarks, $\tilde{q} \to q + \tilde{\chi}_1^0$, or antisquarks, $\bar{\tilde{q}} \to \bar{q} + \tilde{\chi}_1^0$, at NLO is the next necessary step. In this combination we take into account only those contributions to the process $pp \to 2q + 2\tilde{\chi}_1^0$ that lead to two on-shell intermediate squarks. In the narrow width approximation, which is valid in the scenarios analysed here since the widths of the squarks fulfil $\Gamma_{\tilde{q}_i}/m_{\tilde{q}_i} \ll 1$, the differential cross section factorizes into the production cross section times the branching ratios of both squark decays

$$\mathrm{d}\sigma_{\mathrm{tot}} = \mathrm{d}\sigma_{\mathrm{prod}} \frac{\mathrm{d}\Gamma^{\tilde{q}_1 \to \tilde{\chi}_1^0 q}}{\Gamma^{\tilde{q}_1}_{\mathrm{tot}}} \frac{\mathrm{d}\Gamma^{\tilde{q}_2 \to \tilde{\chi}_1^0 q}}{\Gamma^{\tilde{q}_2}_{\mathrm{tot}}}. \tag{20}$$

By applying the narrow width approximation we do not only neglect contributions with off-shell squarks, which are known to be suppressed by $\Gamma_{\tilde{q}_i}/m_{\tilde{q}_i}$, but also non-factorizable higher-order contributions. The latter ones comprise interactions between particles of the production and decay stage or between final-state particles of the two decays. These contributions are expected to be suppressed by $\Gamma_{\tilde{q}_i}/m_{\tilde{q}_i}$ as well [95,96]. Only long-range interactions induced by the exchange of soft gluons could still affect the results of exclusive observables. However, an analysis of these effects is beyond the scope of this publication.

Aiming at a combination of the decays at NLO with the production process at NLO the factors in Eq. (20) have to be replaced by the NLO quantities:

$$\begin{aligned}\mathrm{d}\sigma_{\mathrm{tot}} = (\mathrm{d}\sigma_0 + \alpha_s \mathrm{d}\sigma_1) & \frac{\mathrm{d}\Gamma_0^{\tilde{q}_1 \to \tilde{\chi}_1^0 q} + \alpha_s \mathrm{d}\Gamma_1^{\tilde{q}_1 \to \tilde{\chi}_1^0 q}}{\Gamma^{\tilde{q}_1}_{\mathrm{tot},0} + \alpha_s \Gamma^{\tilde{q}_1}_{\mathrm{tot},1}} \\ & \times \frac{\mathrm{d}\Gamma_0^{\tilde{q}_2 \to \tilde{\chi}_1^0 q} + \alpha_s \mathrm{d}\Gamma_1^{\tilde{q}_2 \to \tilde{\chi}_1^0 q}}{\Gamma^{\tilde{q}_2}_{\mathrm{tot},0} + \alpha_s \Gamma^{\tilde{q}_2}_{\mathrm{tot},1}}.\end{aligned} \tag{21}$$

This expression obviously includes beyond-NLO contributions. In order to strictly consider NLO accuracy it has to be expanded to NLO in α_s. There exist two approaches for this problem, both developed in the context of single and pair production of top quarks [87,97].

In the first approach a Taylor expansion of the full expression is performed. This leads to a formula which is normalized to the LO total widths and subtracts the ratios of the NLO corrections to the total widths over the LO total widths from the first term:

$$\begin{aligned}\mathrm{d}\sigma_{\mathrm{tot}} = & \frac{1}{\Gamma^{\tilde{q}_1}_{\mathrm{tot},0}\Gamma^{\tilde{q}_2}_{\mathrm{tot},0}} \Bigg[\mathrm{d}\sigma_0 \, \mathrm{d}\Gamma_0^{\tilde{q}_1 \to \tilde{\chi}_1^0 q} \, \mathrm{d}\Gamma_0^{\tilde{q}_2 \to \tilde{\chi}_1^0 q} \\ & \times \left(1 - \frac{\alpha_s \Gamma^{\tilde{q}_1}_{\mathrm{tot},1}}{\Gamma^{\tilde{q}_1}_{\mathrm{tot},0}} - \frac{\alpha_s \Gamma^{\tilde{q}_2}_{\mathrm{tot},1}}{\Gamma^{\tilde{q}_2}_{\mathrm{tot},0}} \right) \\ & + \alpha_s \Big(\mathrm{d}\sigma_0 \, \mathrm{d}\Gamma_1^{\tilde{q}_1 \to \tilde{\chi}_1^0 q} \mathrm{d}\Gamma_0^{\tilde{q}_2 \to \tilde{\chi}_1^0 q} \\ & + \mathrm{d}\sigma_0 \, \mathrm{d}\Gamma_0^{\tilde{q}_1 \to \tilde{\chi}_1^0 q} \mathrm{d}\Gamma_1^{\tilde{q}_2 \to \tilde{\chi}_1^0 q} \\ & + \mathrm{d}\sigma_1 \, \mathrm{d}\Gamma_0^{\tilde{q}_1 \to \tilde{\chi}_1^0 q} \mathrm{d}\Gamma_0^{\tilde{q}_2 \to \tilde{\chi}_1^0 q} \Big) \Bigg].\end{aligned} \tag{22}$$

This subtracted term might lead to negative contributions, if the NLO corrections to the total width are positive and large while the corrections to the partial widths are small. However, this expansion has the advantage that the sum over all possible decay channels reproduces the production cross section, i.e. the branching ratios of all subchannels add up to one.

In the second approach only the numerator is expanded in α_s while the NLO total widths are kept in the denominator. This expansion avoids the problem of potentially negative contributions and leads to the expression:

$$\begin{aligned}\mathrm{d}\sigma_{\mathrm{tot}} = & \frac{1}{\Gamma^{\tilde{q}_1}_{\mathrm{tot}}\Gamma^{\tilde{q}_2}_{\mathrm{tot}}} \Big[\mathrm{d}\sigma_0 \, \mathrm{d}\Gamma_0^{\tilde{q}_1 \to \tilde{\chi}_1^0 q} \mathrm{d}\Gamma_0^{\tilde{q}_2 \to \tilde{\chi}_1^0 q} \\ & + \alpha_s \big(\mathrm{d}\sigma_0 \, \mathrm{d}\Gamma_1^{\tilde{q}_1 \to \tilde{\chi}_1^0 q} \mathrm{d}\Gamma_0^{\tilde{q}_2 \to \tilde{\chi}_1^0 q} \\ & + \mathrm{d}\sigma_0 \, \mathrm{d}\Gamma_0^{\tilde{q}_1 \to \tilde{\chi}_1^0 q} \mathrm{d}\Gamma_1^{\tilde{q}_2 \to \tilde{\chi}_1^0 q} \\ & + \mathrm{d}\sigma_1 \, \mathrm{d}\Gamma_0^{\tilde{q}_1 \to \tilde{\chi}_1^0 q} \mathrm{d}\Gamma_0^{\tilde{q}_2 \to \tilde{\chi}_1^0 q} \big) \Big].\end{aligned} \tag{23}$$

In this approach summing over all possible decay channels does not reproduce the production cross section, as the branching ratios do not add up to one, and in this sense unitarity is violated.

In Sect. 4 results for both methods to combine production and decay at NLO, according to Eqs. (22) and (23), will be presented and compared. However, in all other results the Taylor expansion of the cross section, Eq. (22), will be used since in this approach the unitarity of branching ratios is preserved. In the scenarios analysed here the subtracted terms in Eq. (22) are unproblematic, i.e. the NLO corrections to the total decay widths are small (Table 7).

4 Implementation and results

After a brief discussion of the steps required for the implementation of squark production and decay in the Powheg-Box this section summarizes our main findings, including both numerical results at fixed order perturbation theory and after application of different parton showers. Moreover, we present some results for total rates after applying realistic experimental search cuts.

4.1 Implementation in the Powheg-Box

The implementation of squark–antisquark production in the Powheg-Box is essentially identical to the case of squark pair

production, which has been extensively discussed in [54]. Besides several changes in the main code required for the consideration of processes with strongly interacting SUSY particles the process-dependent parts have to be provided, which comprise

- all independent flavour structures contributing to the Born and real channels,
- the Born and the spin/colour-correlated matrix elements squared,
- the finite part of the virtual contributions,
- the real matrix elements squared,
- and the colour flows for the Born configurations.

The implementation of the various subtraction schemes discussed in Sect. 2.2 is rather involved and has been described in detail in [54], too. In essence, we have implemented (besides the two DR schemes) several versions of the DS scheme by splitting the real matrix element squared into a part containing the resonant gluino contributions and the corresponding subtraction terms and a part containing all other terms. The resonant parts do not contain any IR singularities and can therefore be treated independently from the Powheg-like event generation, similar to the 'hard' part $\mathcal{R}_h$ of the real matrix elements squared introduced below.

We have implemented these building blocks for squark–antisquark production into the version 2 (V2) of the Powheg-Box and ported our previous implementation of squark pair production to the V2. This newer version of the Powheg-Box allows for the consideration of NLO corrections to the decays of the on-shell produced squarks. We use this new option to combine our results for the NLO production processes with the corrections to the specific decay $\tilde{q} \to q\tilde{\chi}_1^0$ described in the previous section.[4] Besides taking into account the decay products in the flavour structures as described in the manual of the Powheg-Box V2 this requires the combination of the production and decay matrix elements according to the combination formula in Eq. (22). Moreover, the FKS subtraction of the IR divergences related to the gluon emission off either the squark or the quark in the NLO corrections to the decay process requires the specification of the colour correlated Born matrix elements squared. These are trivial in the case at hand and read in the convention of the Powheg-Box $\mathcal{B}_{\tilde{q}q} = C_F\mathcal{B}$.

In order to check the correctness of the implemented results the same tests as described in [54] have been performed. These comprise a comparison of numerous differential distributions evaluated at NLO with the corresponding results after generation of the hardest emission according to the Powheg method, both at the level of the production processes and after including the decays. While we find an excellent agreement for inclusive quantities, a strong enhancement of the Powheg results compared to the respective NLO distributions is observed for exclusive quantities like the transverse momentum of the squark–antisquark system, $p_T^{\tilde{q}\bar{\tilde{q}}}$. The same artificial enhancement has already been observed in case of squark pair production and can be cured by using the soft/collinear limits of the real matrix elements squared $\mathcal{R}$ instead of the full expressions for the generation of the hardest radiation. In the Powheg-Box this is achieved by introducing a function $\mathcal{F}$ which separates the soft/collinear part $\mathcal{R}_s$ and the hard part $\mathcal{R}_h$ of the real matrix elements squared:

$$\mathcal{R} = \mathcal{F}\mathcal{R} + (1-\mathcal{F})\mathcal{R} \equiv \mathcal{R}_s + \mathcal{R}_h. \tag{24}$$

This function $\mathcal{F}$ has to fulfil $\mathcal{F} \to 1$ in the soft/collinear limit and should vanish far away from the corresponding phase space regions. In the Powheg-Box the functional form

$$\mathcal{F} = \frac{h^2}{p_T^2 + h^2} \tag{25}$$

is used, with the transverse momentum p_T of the emitted parton with respect to the emitter and a damping parameter h (see [57,59] for further details). Similar to our earlier studies on squark pair production we use $h = 50\,\text{GeV}$ throughout. This choice was found to damp the artificial enhancement in the $p_T^{\tilde{q}\bar{\tilde{q}}}$ distribution and reproduces the NLO prediction for $p_T^{\tilde{q}\bar{\tilde{q}}} \gtrsim 200\,\text{GeV}$, while maintaining the Sudakov damping for small transverse momenta inherent in the Powheg method.[5]

4.2 Setup

For the numerical analysis we consider two mSUGRA scenarios which are not yet excluded by data, see e.g. [99,100]. The scenarios are based on the CMSSM points 10.3.6*[6] and 10.4.5 from [84]. The input parameters of these scenarios are summarized in Table 2. The mass spectrum of the SUSY particles has been generated with Softsusy 3.3.4 [101], the resulting on-shell masses are then used as input parameters. For the SM parameters the following values are used [92]:

[4] In [98] the Powheg formalism was already used to improve the simulation of the hard radiation in beyond SM decays, including $\tilde{u}_L \to u\tilde{\chi}_1^0$, in the Herwig++ event generator. However, since this work focuses on the effect of the Powheg correction on the simulation of the hardest emission, the normalization to NLO accuracy, requiring also the virtual corrections, could not be taken into account.

[5] A detailed discussion on the impact of different values of the damping parameter h for squark pair production can be found in [54] and for squark–antisquark production in [56].

[6] For the point 10.3.6 m_0 has been modified to get a mass spectrum consistent with the latest exclusion bounds.

Table 2 The input parameters for the considered scenarios

Scenario	m_0 (GeV)	$m_{1/2}$ (GeV)	A_0 (GeV)	$\tan(\beta)$	$\mathrm{sgn}(\mu)$
10.3.6*	825	550	0	10	+1
10.4.5	1150	690	0	10	+1

Table 3 The squark masses in GeV obtained with the parameters from Table 2 after averaging the masses of the first two generations as described in the text

Scenario	$m_{\tilde{u}_L} = m_{\tilde{c}_L}$	$m_{\tilde{u}_R} = m_{\tilde{c}_R}$	$m_{\tilde{d}_L} = m_{\tilde{s}_L}$	$m_{\tilde{d}_R} = m_{\tilde{s}_R}$	$m_{\tilde{g}}$
10.3.6*	1799.53	1760.21	1801.08	1756.40	1602.96
10.4.5	1746.64	1684.31	1748.25	1677.82	1840.58

$$m_Z = 91.1876\,\mathrm{GeV}, \quad G_F = 1.16637 \times 10^{-5}\,\mathrm{GeV}^{-2},$$
$$\alpha_{em}(m_Z) = 1/127.934, \quad \alpha_s(m_Z) = 0.118,$$
$$m_b^{\overline{\mathrm{MS}}}(m_b) = 4.25\,\mathrm{GeV}, \quad m_t = 174.3\,\mathrm{GeV},$$
$$m_\tau = 1.777\,\mathrm{GeV}, \quad m_c^{\overline{\mathrm{MS}}}(m_c) = 1.27\,\mathrm{GeV}. \tag{26}$$

As Softsusy implements non-vanishing Yukawa corrections, there is a small difference between the masses of the second-generation squarks and the corresponding first-generation ones, i.e. $m_{\tilde{u}_L} \neq m_{\tilde{c}_L}$ etc. To simplify the analysis and save computing time these masses are replaced by the mean of the mass pairs, i.e. $m_{\tilde{u}_L}$ and $m_{\tilde{c}_L}$ are replaced by $(m_{\tilde{u}_L} + m_{\tilde{c}_L})/2$ and so on. The obtained masses for the squarks of the first two generations and the gluino masses are summarized in Table 3. Note that for the point 10.3.6* the mass hierarchy is $m_{\tilde{q}} > m_{\tilde{g}}$, while for 10.4.5 $m_{\tilde{q}} < m_{\tilde{g}}$, the latter point requiring the subtraction of contributions with on-shell intermediate gluinos as described in Sect. 2.2. Here, the DS* method is used, with a default value for the regulator $\Gamma_{\tilde{g}} = 1\,\mathrm{GeV}$ (recall that this regulator is only needed if a subtraction is required, thus in all other cases it is set to zero).

Furthermore, the partial and total decay widths of the squarks depend on the masses of the charginos and neutralinos and the respective mixing matrices. The masses of the neutralinos and charginos for the two scenarios are given in Table 4. The neutralino mixing matrices for the scenarios 10.3.6* and 10.4.5 read

$$N^{10.3.6*} = \begin{pmatrix} 0.99759 & -0.00979 & 0.06292 & -0.02740 \\ 0.02329 & 0.97889 & -0.16595 & 0.11704 \\ -0.24682 & 0.03551 & 0.70512 & 0.70776 \\ -0.06044 & 0.20106 & 0.68651 & -0.69615 \end{pmatrix} \quad \text{and}$$
$$N^{10.4.5} = \begin{pmatrix} 0.98267 & -0.00716 & 0.05338 & -0.02358 \\ -0.20847 & 0.02997 & 0.70567 & 0.70760 \\ 0.01724 & 0.98393 & -0.14473 & 0.10318 \\ -0.05226 & 0.17590 & 0.69154 & -0.69865 \end{pmatrix}. \tag{27}$$

Table 4 The neutralino and chargino masses for the benchmark scenarios defined in Table 2

Scenario	$m_{\tilde{\chi}_1^0}$ (GeV)	$m_{\tilde{\chi}_2^0}$ (GeV)	$m_{\tilde{\chi}_3^0}$ (GeV)	$m_{\tilde{\chi}_4^0}$ (GeV)	$m_{\tilde{\chi}_1^\pm}$ (GeV)	$m_{\tilde{\chi}_2^\pm}$ (GeV)
10.3.6*	290.83	551.76	−844.74	856.87	551.99	856.40
10.4.5	347.71	657.84	−993.42	1003.79	856.06	1003.46

In order to diagonalize the chargino mass matrix two matrices are needed, one for the left-handed components (denoted U) and one for the right-handed ones (denoted V). These 2×2 mixing matrices are parametrized as ($i = U, V$)

$$\begin{pmatrix} \cos\theta_i & -\sin\theta_i \\ \sin\theta_i & \cos\theta_i \end{pmatrix}. \tag{28}$$

The mixing angles are given by $\cos\theta_U = 0.97213$ and $\cos\theta_V = 0.98594$ for the parameter point 10.3.6*. Likewise, those for the scenario 10.4.5 read $\cos\theta_U = 0.97894$ and $\cos\theta_V = 0.98914$.

The renormalization (μ_R) and factorization (μ_F) scales are chosen as $\mu_R = \mu_F = \overline{m}_{\tilde{q}}$, with $\overline{m}_{\tilde{q}}$ representing the average of the squark masses of the first two generations. For the two scenarios defined above one obtains $\overline{m}_{\tilde{q}}^{10.3.6*} = 1779.31\,\mathrm{GeV}$ and $\overline{m}_{\tilde{q}}^{10.4.5} = 1714.25\,\mathrm{GeV}$, respectively. All subchannels for the production of first- and second-generation squarks are taken into account for the results, i.e. if not stated otherwise all results presented in the rest of this section are obtained by adding up the subchannels. For squark pair production the (tiny) contributions of the antisquark pair production channels are always taken into account.

The PDFs are taken from the LHAPDF package [102]. For the LO results shown in the following the LO set CTEQ6L1 [103] with $\alpha_s(m_Z) = 0.130$ is used, while the NLO results are calculated with the NLO set CT10NLO with $\alpha_s(m_Z) = 0.118$ [104]. The strong coupling constant for the LO results is correspondingly computed using the one-loop renormalization group equations, while the value used in the NLO results is obtained from the two-loop equations.

All results are calculated for the LHC with $\sqrt{s} = 14\,\mathrm{TeV}$. The error bars shown in the following represent the statistical errors of the Monte Carlo integration.

Taking into account the decays of the produced squarks into $q\tilde{\chi}_1^0$ or applying a parton shower algorithm leads to a potentially large number of partons in the final state. These partons are clustered into jets with Fastjet 3.0.3 [105,106]. To this end the anti-k_T algorithm [107] is adopted, using $R = 0.4$. In the following only minimal cuts are applied on the transverse momentum and the pseudorapidity of the resulting jets:

$$p_T^j > 20\,\mathrm{GeV} \quad \text{and} \quad |\eta^j| < 2.8. \tag{29}$$

Table 5 The LO and NLO cross sections for squark–antisquark production for the two benchmark scenarios defined in Sect. 4.2. The theoretical error estimates $\pm\Delta\sigma$ have been obtained by varying the renormalization and factorization scales by a factor two around the central values

Scenario	$\sigma_{\text{LO}}^{\pm\Delta\sigma}$ (fb)	$\sigma_{\text{NLO}}^{\pm\Delta\sigma}$ (fb)	K-factor
10.3.6*	$2.319^{+34\,\%}_{-24\,\%}$	$3.218^{+13\,\%}_{-14\,\%}$	1.39
10.4.5	$3.098^{+34\,\%}_{-24\,\%}$	$4.366^{+14\,\%}_{-14\,\%}$	1.41

Except for the results shown in Sect. 4.3.3 no event selection cuts are imposed.

4.3 Numerical results

4.3.1 Results at fixed order

The first part of this section is devoted to a discussion of the NLO corrections to squark–antisquark production. In the second part we present some results for the combination of production and decay, both for squark–antisquark and squark pair production. Hence this part extends our previous results for the squark pair production processes in [54] by also including the NLO corrections to the decay.

Squark–antisquark production

The results for the total squark–antisquark production cross sections determined at LO and NLO for the two benchmark scenarios defined in Sect. 4.2 are summarized in Table 5. In order to assess the theoretical uncertainties we vary the renormalization and factorization scales by a factor two around the central value $\mu = \overline{m}_{\tilde{q}}$. The resulting percental uncertainties are also given in the table. Considering the resulting K-factors we note that in both cases the SUSY-QCD NLO corrections are positive and large, resulting in $K \equiv \sigma_{\text{NLO}}/\sigma_{\text{LO}} \approx 1.4$. The scale uncertainties are strongly reduced by taking into account the NLO corrections, as expected.

Turning next to the individual K-factors for the subchannels contributing to squark–antisquark production we observe that they differ significantly from the total K-factor obtained after summing the cross sections for all individual channels. To illustrate this point, the LO/NLO cross sections and the resulting K-factors for the production channels involving only squarks of the first generation are given in Table 6 for the CMSSM point 10.3.6*. Note, that the channels with squarks of the same flavour and chirality in the final state, displayed in the first four rows of the table, have contributions from gg initial states and therefore larger K-factors than channels with squarks of different flavour or chirality. Hence the assumption that the individual K-factors can be approximated by the total K-factor obtained from Prospino is in general not valid.

Table 6 The LO and NLO cross sections for squark–antisquark production of the first generation obtained for the CMSSM point 10.3.6*. The charge conjugate channels have been combined

Process	σ_{LO} (fb)	σ_{NLO} (fb)	K-factor
$\tilde{u}_{\text{L}}\bar{\tilde{u}}_{\text{L}}$	9.51×10^{-2}	1.43×10^{-1}	1.50
$\tilde{u}_{\text{R}}\bar{\tilde{u}}_{\text{R}}$	1.14×10^{-1}	1.72×10^{-1}	1.51
$\tilde{d}_{\text{L}}\bar{\tilde{d}}_{\text{L}}$	5.50×10^{-2}	8.79×10^{-2}	1.60
$\tilde{d}_{\text{R}}\bar{\tilde{d}}_{\text{R}}$	6.89×10^{-2}	1.11×10^{-1}	1.61
$\tilde{u}_{\text{L}}\bar{\tilde{u}}_{\text{R}}$	3.75×10^{-1}	5.12×10^{-1}	1.37
$\tilde{d}_{\text{L}}\bar{\tilde{d}}_{\text{R}}$	1.41×10^{-1}	1.70×10^{-1}	1.21
$\tilde{u}_{\text{L}}\bar{\tilde{d}}_{\text{L}}$	6.98×10^{-2}	7.89×10^{-2}	1.13
$\tilde{u}_{\text{L}}\bar{\tilde{d}}_{\text{R}}$	2.98×10^{-1}	3.54×10^{-1}	1.19
$\tilde{u}_{\text{R}}\bar{\tilde{d}}_{\text{L}}$	2.94×10^{-1}	3.49×10^{-1}	1.19
$\tilde{u}_{\text{R}}\bar{\tilde{d}}_{\text{R}}$	8.36×10^{-2}	9.54×10^{-2}	1.14
Sum	1.59	2.07	1.30

Determining the individual corrections consistently is especially important if the decays are taken into account and the branching ratios of the different squarks differ significantly for the specific decay channel under consideration. In order to assess the possible numerical impact of this approximation we consider the decay $\tilde{q} \to q\tilde{\chi}_1^0$ at LO at the level of total cross sections, i.e. we multiply the production cross sections for the individual squark–antisquark production channels with the respective LO branching ratios. In this step we take into account the contributions of the second generation squarks as well.

We first consider the benchmark scenario 10.3.6*. Using the correctly calculated NLO results for the individual production channels, multiplying them with the corresponding branching ratios and summing all channels, we obtain

$$\sum_{\text{channels}} \sigma_{\text{NLO}} \cdot \text{BR}^{\text{LO}}\left(\tilde{q} \to \tilde{\chi}_1^0 q\right) \cdot \text{BR}^{\text{LO}}\left(\bar{\tilde{q}} \to \tilde{\chi}_1^0 \bar{q}\right) = 0.139\,\text{fb}. \tag{30}$$

To mimic the way Prospino obtains the individual NLO results a common K-factor has to be calculated, using an averaged squark mass $m_{\tilde{q}} = 1779.31\,\text{GeV}$. In the case at hand this leads to

$$\sigma_{\text{LO}}^{\text{avg}} = 2.315\,\text{fb}, \quad \sigma_{\text{NLO}}^{\text{avg}} = 3.218\,\text{fb} \Rightarrow K^{\text{avg}} = 1.39. \tag{31}$$

Note that the difference compared to the full calculation given in Table 5 is marginal and not visible when rounding to the second decimal place. This is due to the fact that the spread in the squark masses is rather small. Multiplying the LO result for each subchannel with this common K-factor and the corresponding branching ratios gives

Table 7 The total widths for first-generation squarks at LO and NLO for the two scenarios considered here. The widths for the second-generation squarks are identical. For the parameters see the main text. The scale for α_s has been set to $\mu_R = \overline{m}_{\tilde{q}}$

	10.3.6*		10.4.5	
	Γ_{LO} (GeV)	Γ_{NLO} (GeV)	Γ_{LO} (GeV)	Γ_{NLO} (GeV)
$\tilde{u}_L$	22.79	23.44	16.21	15.81
$\tilde{u}_R$	6.561	7.413	3.493	3.411
$\tilde{d}_L$	22.78	23.45	16.14	15.74
$\tilde{d}_R$	3.610	4.553	0.869	0.849

$$\sum_{\text{channels}} \sigma_{LO} \cdot K^{\text{avg}} \cdot \text{BR}^{LO}\left(\tilde{q} \to \tilde{\chi}_1^0 q\right) \cdot \text{BR}^{LO}\left(\bar{\tilde{q}} \to \tilde{\chi}_1^0 \bar{q}\right) = 0.126\,\text{fb}. \quad (32)$$

Thus the rate obtained with the approximation relying on a constant K-factor for all subchannels is roughly 10 % smaller for this special case.

Repeating this procedure for the benchmark scenario 10.4.5 one obtains for the Prospino-like K-factor

$$\sigma_{LO}^{\text{avg}} = 3.090\,\text{fb}, \quad \sigma_{NLO}^{\text{avg}} = 4.356\,\text{fb} \Rightarrow K^{\text{avg}} = 1.41. \quad (33)$$

Again, comparing this result to the full calculation given in Table 5 the discrepancy is only marginal.

Considering the individual subchannels with the correct individual NLO corrections yields

$$\sum_{\text{channels}} \sigma_{NLO} \cdot \text{BR}^{LO}\left(\tilde{q} \to \tilde{\chi}_1^0 q\right) \cdot \text{BR}^{LO}\left(\bar{\tilde{q}} \to \tilde{\chi}_1^0 \bar{q}\right) = 0.916\,\text{fb}, \quad (34)$$

while the approximation of the common K-factor gives

$$\sum_{\text{channels}} \sigma_{LO} \cdot K^{\text{avg}} \cdot \text{BR}^{LO}\left(\tilde{q} \to \tilde{\chi}_1^0 q\right) \cdot \text{BR}^{LO}\left(\bar{\tilde{q}} \to \tilde{\chi}_1^0 \bar{q}\right) = 0.807\,\text{fb} \quad (35)$$

and thus again a discrepancy of about 10 %.

Squark production and decay at NLO

As discussed in Sect. 3.3 we have used two different approaches to combine the production and decay processes at NLO, differing in the way the combined expression is expanded in α_s. Both approaches require the calculation of the total squark width, either at LO or NLO accuracy. The results for the two considered benchmark scenarios are summarized in Table 7.

In a first step we compare the numerical results obtained with these approaches, both for differential distributions and total cross sections. In Fig. 6 the distributions for the transverse momenta of the hardest and the second hardest jet, $p_T^{j_1/j_2}$, their invariant mass $m^{j_1 j_2}$ and the missing transverse energy $\not{E}_T$ are depicted for squark–antisquark production using the benchmark scenario 10.3.6*. Here, App. 1 corresponds to the Taylor expansion according to Eq. (22), whereas in App. 2 only the numerator in the combination formula is expanded, see Eq. (23).

The discrepancies between the approaches 1 and 2 can amount to up to $\mathcal{O}(15\,\%)$ for the jet distributions and are largest close to threshold, while the results for $\not{E}_T$ reflect only the overall discrepancy in the total cross sections, which amounts for this scenario to approximately 4 %.

The total cross sections for the combined production and decay processes as obtained with both approaches are summarized in Table 8, both for the scenario 10.3.6* and 10.4.5. Note that the predictions for the LO cross sections are identical in both approaches and have been calculated according to Eq. (20) using the LO quantities. Comparing the results for the different predictions at NLO reveals only rather small discrepancies <4 % for the total rates for the scenarios considered here. In the rest of this chapter we use exclusively the first approach to combine production and decay processes.

In order to assess the influence of the NLO corrections on differential cross sections we consider in the following the differential K-factors for several observables. In Fig. 7 the LO and the NLO distributions for the transverse momentum of the hardest jet, $p_T^{j_1}$, its rapidity, y^{j_1}, the missing transverse energy $\not{E}_T$ and the effective mass $m_{\text{eff}} \equiv p_T^{j_1} + p_T^{j_2} + \not{E}_T$ are depicted for squark–antisquark production, using the benchmark scenario 10.3.6*. The results for the scenario 10.4.5 are qualitatively the same. Considering the p_T distribution of the hardest jet one observes a strong enhancement of the NLO corrections for small values of p_T, while they turn even negative for large values. The result for the second hardest jet, which is not shown here, is qualitatively the same. A similar observation holds for the effective mass: the NLO curve is dragged to smaller values of m_{eff} and the differential K-factor depicted in the lower panel is far from being flat over the whole region. For the $\not{E}_T$ predictions, in contrast, the deviation of the differential K-factor from the total one is rather small, of $\mathcal{O}(5\,\%)$, except for events with very small or very large missing transverse energy. Likewise, the shape of the rapidity distribution of the hardest jet is hardly affected by the NLO corrections.

Next we consider the same set of distributions for squark pair production with subsequent decays, this time for the scenario 10.4.5, depicted in Fig. 8. Again the results for 10.3.6* are qualitatively identical and not shown here. In essence, the behaviour is very much the same as for squark–antisquark production in Fig. 7 and differs only in details. For example the differential K-factor of the rapidity distribution y^{j_1} shows

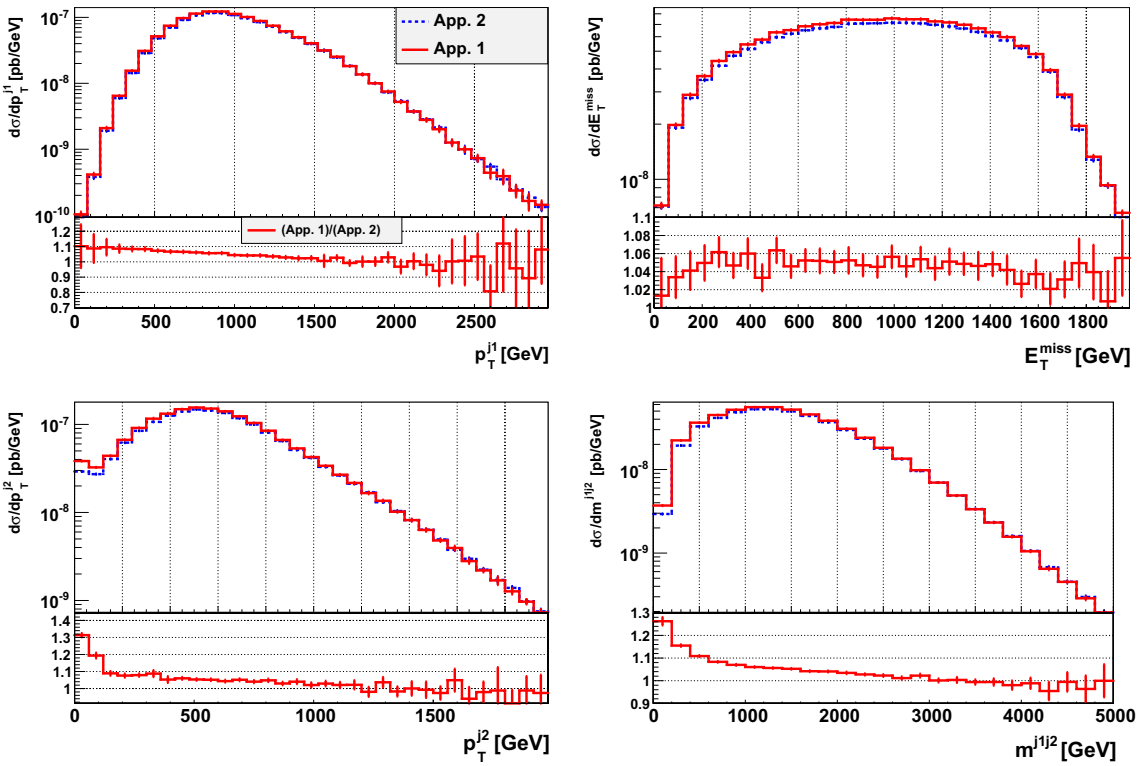

Fig. 6 Comparison of the two approaches specified in the text for the combination of NLO corrections in production and decay. Shown are the distributions obtained for squark–antisquark production and subsequent decays for the scenario 10.3.6*. The *lower panels* show the differential ratios of the first approach with respect to the second approach

Table 8 Cross sections for squark production and decay at LO and NLO, combined according to Eq. (22) (App. 1) and Eq. (23) (App. 2)

Scenario	10.3.6*			10.4.5		
Process	σ_{LO}(fb)	σ_{NLO}(fb)	K-factor	σ_{LO}(fb)	σ_{NLO}(fb)	K-factor
$\tilde{q}\tilde{q}$-App. 1	1.34	1.12	0.84	7.57	8.75	1.16
$\tilde{q}\tilde{q}$-App. 2	1.34	1.09	0.81	7.57	8.89	1.17
$\tilde{q}\bar{\tilde{q}}$-App. 1	9.29×10^{-2}	1.03×10^{-1}	1.11	5.73×10^{-1}	9.15×10^{-1}	1.60
$\tilde{q}\bar{\tilde{q}}$-App. 2	9.29×10^{-2}	9.88×10^{-2}	1.06	5.73×10^{-1}	9.32×10^{-1}	1.63

slightly larger deviations from the total K-factor, whereas the one for $\not{E}_T$ is a bit flatter in the range considered here.

4.3.2 Parton shower effects

In order to investigate parton shower effects we have combined our implementations of the squark production and decay processes with different parton shower programs. To this end five million events have been generated for squark–antisquark and squark pair production for each of the two benchmark scenarios defined in Sect. 4.2. The results shown in the following have been obtained by setting the folding parameters of the Powheg-Box to the values

$$n_\xi = 5, \quad n_y = 5, \quad n_\phi = 1, \tag{36}$$

reducing such the number of events with negative weights. However, in the context of squark production and decay processes two further sources of negative events can occur. The first one originates from the way production and decay are combined in Eq. (22), see the discussion in Sect. 3.3. It is not possible to apply the folding procedure described above in this case, since the negative contributions to $\overline{\mathcal{B}}$ are directly related to the (modified) Born contribution. Using a different expansion of the combination formula, e.g. Eq. (23), would remedy this point, however this approach violates unitarity and should therefore be avoided.

The implemented subtraction schemes described in Sect. 2.2 present another source of contributions with negative weights. While these are completely absent for the DR-I method and their number can be reduced again by means

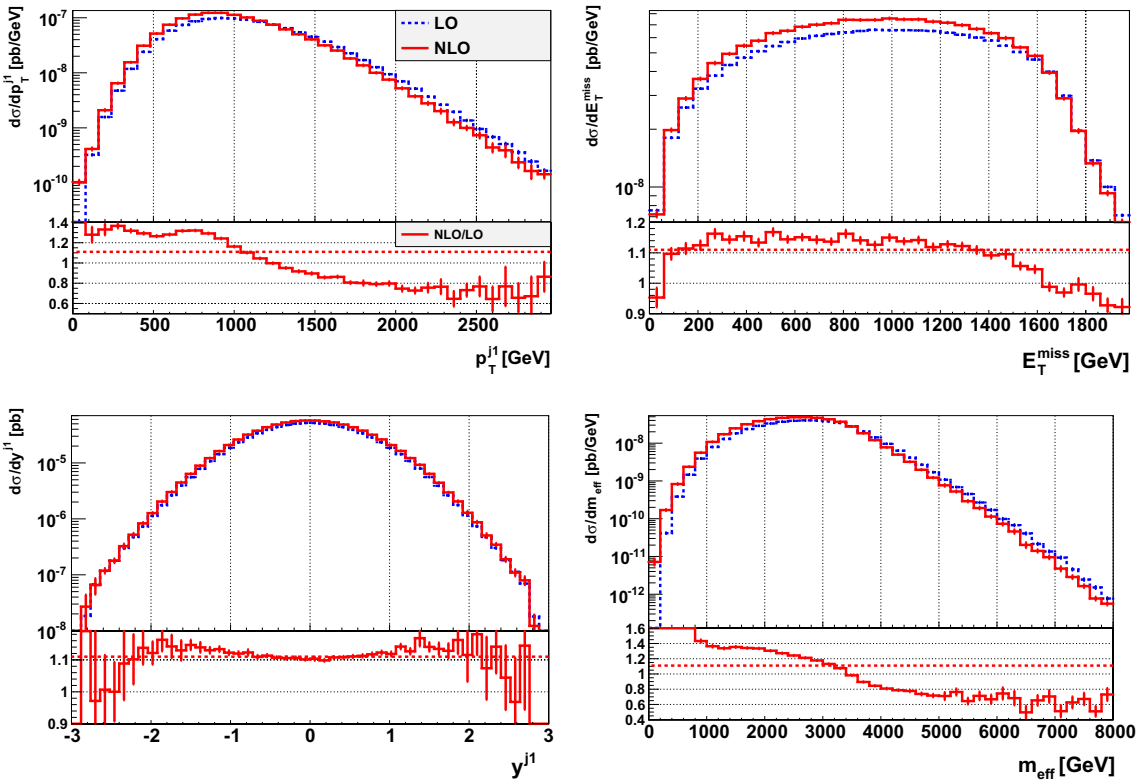

Fig. 7 Differential distributions as defined in the text for squark–antisquark production, combined with the subsequent decay $\tilde{q} \to q\tilde{\chi}_1^0$ and the corresponding decay for the antisquark for the scenario 10.3.6*. Shown are the LO predictions obtained using Eq. (20) and the NLO results determined according to Eq. (22). In all plots the *lower panels* depict the respective differential K-factor (*full*) and the total K-factor from Table 8 (*dashed*)

of folding for the DS* and the DR-II method, they inevitably occur for the methods relying on a splitting of $\mathcal{R}$.

All in all, using the (for conceptual reasons preferable) DS* subtraction scheme with split real matrix elements squared and Eq. (22) for the combination of production and decay leads unavoidably to events with negative weights, which cannot be neglected. Therefore, they are kept in the generated event files by setting the Powheg-Box flag `withnegweights` = 1.

The generated event samples have been showered with two Monte Carlo event generators, using three different parton shower algorithms implemented in these programs:

- *Pythia 6* We use the version 6.4.28 [108]. All results have been obtained with the Perugia 0 tune [109], invoked by setting `MSTP(5) = 320`. A comparison with the Perugia 11 tune (`MSTP(5) = 350`) yields only tiny discrepancies.[7] In order to study only effects of the parton shower, hadronization and multi-parton interaction (MPI) effects have been turned off by setting `MSTP(111) = 0` and `MSTP(81) = 20`, invoking thus the use of the p_T-ordered shower.
However, in the simulation of the full process, including NLO corrections to the production and the decays, a further subtle difficulty arises when using Pythia, which is related to the way the starting scales for the shower are chosen. The Powheg approach relies on the assumption that the p_T of the emitted final-state parton is larger than the transverse momentum of any subsequent splitting generated by the parton shower. This requires the application of a p_T veto in the parton shower, with the maximal scale being read for each event from the event file. However, if final-state resonances are present the mass of those has to be preserved by the reshuffling operations performed in the shower algorithm. Therefore, the showering of partons originating from the decays of these resonances, i.e. in the processes considered here the produced squarks, is performed separately in Pythia. The starting scale for these shower contributions is set to the invariant mass of all decay products, hence in the case at hand to the mass of the respective squark. In the scenarios considered here this scale is typically an order of magnitude larger than the upper scale written to the event file,

[7] To be more precise, for squark–antisquark production, including the decays and using the benchmark scenario 10.3.6*, of all observables considered in this section only the $p_T^{j_3}$ distribution shows with $\mathcal{O}(5\,\%)$ a deviation larger than 1 %.

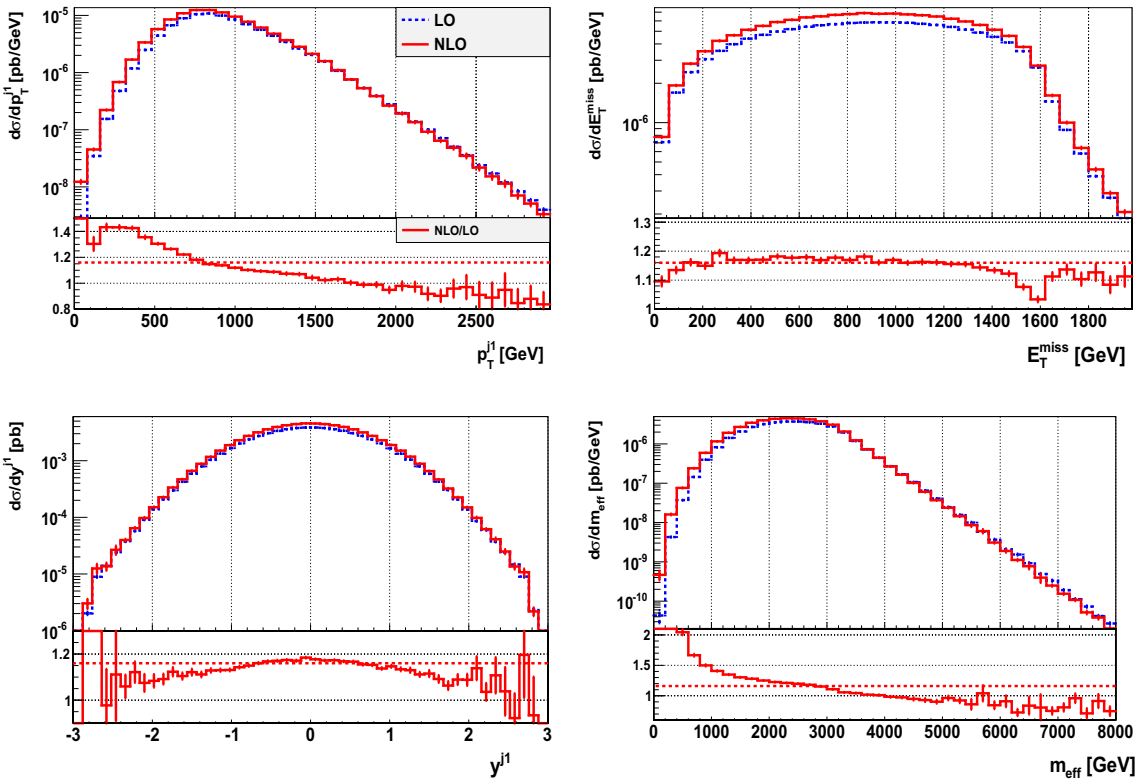

Fig. 8 Same as Fig. 7 for squark pair production and the scenario 10.4.5

leading to much more radiation and thus to a strong bias of the results. In order to correct for this effect, the Pythia routines had to be adapted to use the scale specified in the event file as starting scale in all individual contributions to the parton shower.

- *Herwig++* The default shower of Herwig++ [110] is ordered in the angles of the branchings. Applying this shower to an event sample generated according to the Powheg method requires again the use of a p_T veto. However, this combination lacks the emission of soft wide-angle partons, as the first emission in an angular-ordered shower is not necessarily the hardest one. In principle these missing parts have to be simulated in an extra step via a so-called vetoed truncated shower, which is not provided by Herwig++ and thus not taken into account in the following. The effect of this missing part will be estimated by comparing the results to those obtained with the p_T-ordered Dipole-Shower [111,112], which is also part of the Herwig++ framework. The results presented in the following sections have been obtained using the version 2.6.1 [113]. In the following Herwig++ refers only to the default shower, while the results labeled Dipole-shower or, for the sake of brevity, Dipole refer to the Dipole-shower included in the Herwig++ framework.

The showered results for squark–antisquark production are shown in Fig. 9, using the scenario 10.3.6*. Likewise, Fig. 10 depicts the results for squark pair production, obtained with the scenario 10.4.5. All plots show the outcome of the three parton showers described above and the NLO prediction, which serves as normalization in the ratio plots shown in the lower panels. The results for squark pair production using scenario 10.3.6* and squark–antisquark production with scenario 10.4.5 do not reveal any new features compared to the depicted combinations and are therefore not shown here.

Comparing the predictions for the individual observables shown in the two figures we note that in all cases considered here the $p_T^{j_1}$ result obtained with Herwig++ is in the low-p_T region slightly [$\mathcal{O}(10\,\%)$] enhanced compared to the other parton showers, whereas the Dipole-shower and Pythia essentially agree here. At the other end of the spectrum, however, both the Herwig++ and the Dipole-shower predict $\mathcal{O}(10\,\%)$ smaller rates than Pythia, which is almost in accordance with the NLO result for large values of $p_T^{j_1}$. The outcome of Herwig++ and the Dipole-shower is identical in this kinematic regime. Similar conclusions can be drawn from the $p_T^{j_2}$ and the $m^{j_1 j_2}$ distributions. In contrast, the distributions describing the third hardest jet show more pronounced differences. Comparing first the results for $p_T^{j_3}$

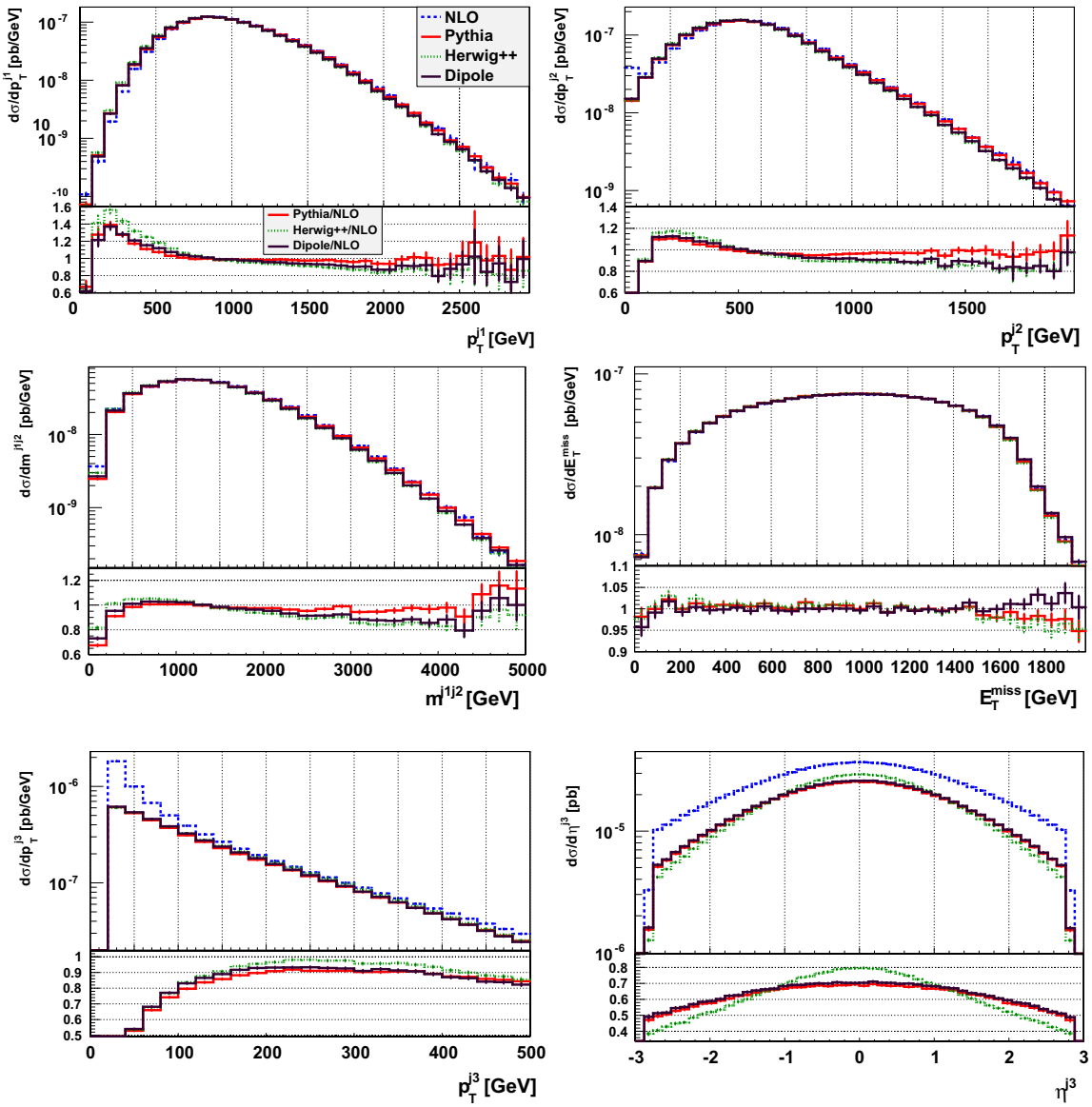

Fig. 9 Differential distributions for squark–antisquark production, combined with the subsequent decay $\tilde{q} \to q\tilde{\chi}_1^0$ for the scenario 10.3.6*. The NLO predictions and the results after applying the parton showers Pythia, Herwig++and the Dipole-shower are shown. In all plots the *lower panels* depict the respective ratios of the results obtained with the three parton showers and the pure NLO prediction

obtained with Herwig++ and the Dipole-shower one notices that they agree within $\mathcal{O}(5\text{–}10\,\%)$. The result for the third jet obtained with Pythia is in all cases smaller compared to the other two parton showers. While the discrepancy using the benchmark scenario 10.3.6* is for both squark–antisquark and squark pair production smaller than 10 %, it amounts to 10–15 % for the scenario 10.4.5 in both cases. In both scenarios and production channels all parton showers predict $\mathcal{O}(20\,\%)$ smaller rates than the pure NLO simulation for large values of $p_T^{j_3}$. Since the NLO prediction is reproduced in this region when considering only the first radiation generated according to the Powheg method [54,56], this softening behaviour is caused by additional radiation generated in the showering stage. The largest differences in the three shower predictions emerge in the results for the pseudorapidity of the third hardest jet, η^{j_3}. While Pythia and the Dipole-shower agree within 5 % for all cases and differ in case of squark pair production only in the overall normalization, but not in the shape of the distributions, Herwig++ predicts evidently more jets in the central region $\left|\eta^{j_3}\right| \lesssim 1$. Comparing the Herwig++ result and the Pythia outcome for squark–antisquark production, this enhancement amounts to a 20 % higher rate in the centre and a reduction of the same magnitude for $\left|\eta^{j_3}\right| \approx 2.8$. In case of squark pair production, this effect is smaller, of $\mathcal{O}(10\,\%)$, but still clearly visible. The predictions for the missing transverse energy $\not{E}_T$ agree very

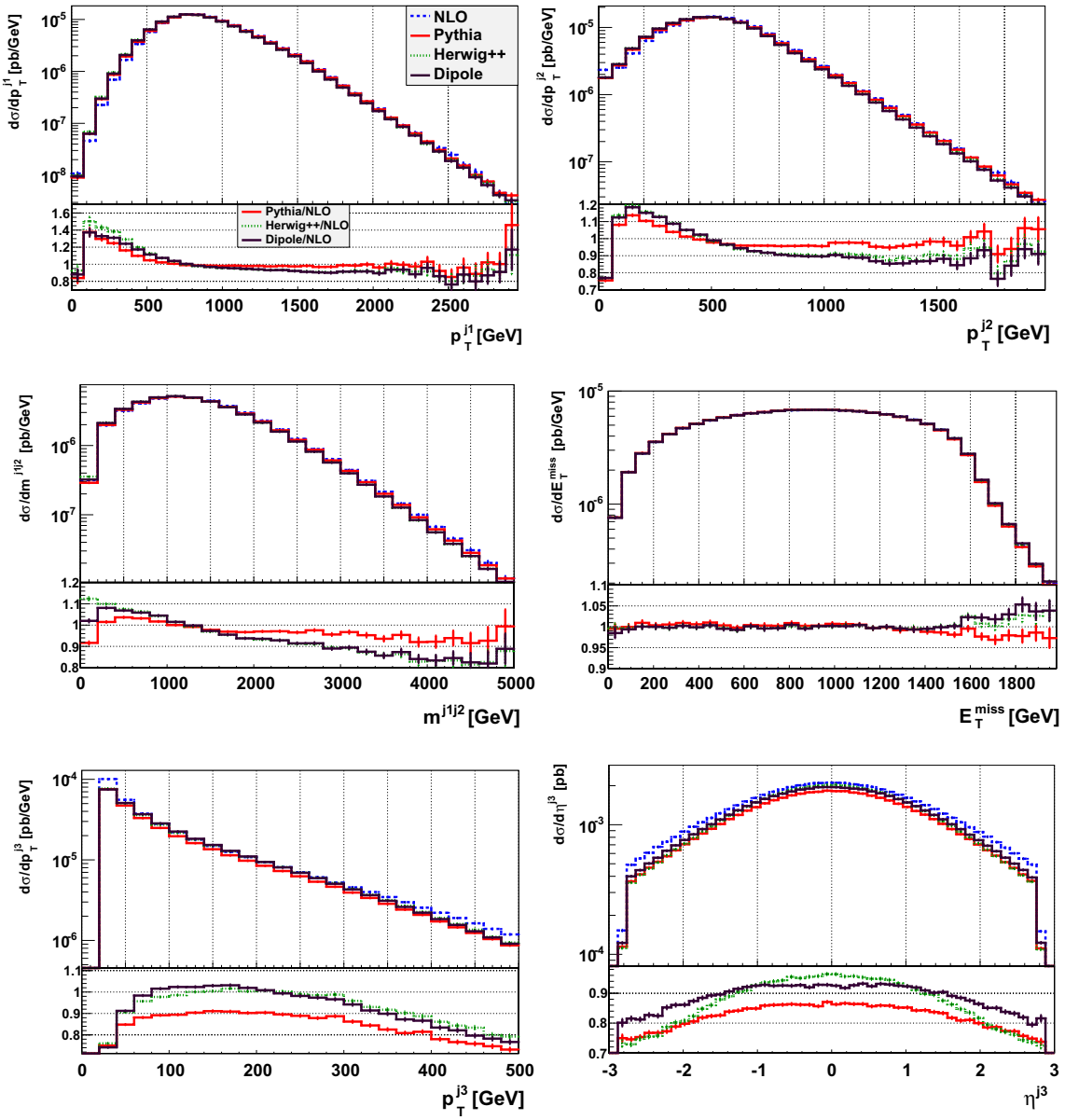

Fig. 10 Same as Fig. 9 for squark pair production and the benchmark scenario 10.4.5

well and essentially reproduce the NLO result. Tiny deviations are only visible in the tails of the distributions, however they are smaller than 5 % in all cases.

All in all, the predictions of the different parton showers for the observables depending solely on the two hardest jets agree within $\mathcal{O}(10\,\%)$ or better. Comparing the showered results with the outcome of a pure NLO simulation the effects of the parton showers on these observables are at most of $\mathcal{O}(10\text{–}20\,\%)$, except for the threshold region. By and large, the two Herwig++ showers yield larger deviations from the NLO outcome for these observables, whereas Pythia reproduces the NLO curves within $\mathcal{O}(10\,\%)$. The $\not{E}_T$ distribution is in all cases hardly affected by parton shower effects. Larger deviations between the different parton showers emerge in the predictions for the third hardest jet, which is formally described only at LO in the hard process. Especially the Herwig++ prediction differs significantly from the other two showers and predicts more jets in the central region of the detector. At this point it is not possible to decide ultimately if this discrepancy is an effect of the missing truncated shower or simply a relict of the way the phase space is populated in the different shower algorithms. This would require the actual implementation of a vetoed truncated shower, which is beyond the scope of this work. However, comparing the outcomes of the Dipole-shower and Herwig++ reveals only very small discrepancies in other observables. Hence the overall effect of the neglected truncated shower seems to be small.

Table 9 Total cross sections after applying the event selection cuts defined in Eq. (37) for the different production modes in the two benchmark scenarios. The decays of the squarks (antisquarks) to $q\tilde{\chi}_1^0$ ($\bar{q}\tilde{\chi}_1^0$) are included at NLO. The given results have been obtained at the level of a pure NLO simulation and including parton shower effects with Pythia and Herwig++, respectively. The last two rows have been obtained by rescaling LO events after application of the Pythia/Herwig++ shower with the constant K-factor and the individual NLO branching ratios

	10.3.6*		10.4.5	
	$\tilde{q}\tilde{q}$ (fb)	$\tilde{q}\bar{\tilde{q}}$ (fb)	$\tilde{q}\tilde{q}$ (fb)	$\tilde{q}\bar{\tilde{q}}$ (fb)
NLO	0.871	0.0781	6.809	0.696
Pythia	0.883	0.0797	6.854	0.704
Herwig++	0.895	0.0807	6.936	0.711
Pythia (approx.)	0.855	0.0664	6.844	0.617
Herwig++ (approx.)	0.858	0.0667	6.876	0.620

4.3.3 Total rates

In the last step the created event samples are analysed using a realistic set of event selection cuts, which corresponds to the definition of the signal region 'A-loose' for the SUSY searches in two-jet events performed by the ATLAS collaboration [99].

The event selection cuts used in this analysis are

$$\begin{aligned} &p_T^{j_1} > 130\,\text{GeV}, \quad p_T^{j_2} > 60\,\text{GeV}, \quad \not{E}_T > 160\,\text{GeV}, \\ &\frac{\not{E}_T}{m_{\text{eff}}} > 0.2, \quad m_{\text{eff}}^{\text{incl}} > 1\,\text{TeV}, \\ &\Delta\phi(j_{1/2}, \not{E}_T) > 0.4, \quad \Delta\phi(j_3, \not{E}_T) > 0.4 \quad \text{if } p_T^{j_3} > 40\,\text{GeV}. \end{aligned} \tag{37}$$

Here, the effective mass m_{eff} is defined as the sum of the p_T of the two hardest jets and $\not{E}_T$, whereas the inclusive definition of this observable includes all jets with $p_T^j > 40\,\text{GeV}$,

$$m_{\text{eff}}^{\text{incl}} = \sum_{i=1}^{n_j} p_T^{j_i} + \not{E}_T. \tag{38}$$

Moreover, $\Delta\phi(j_i, \not{E}_T)$ denotes the minimal azimuthal separation between the direction of the missing transverse energy, $\not{E}_T$, and the ith jet. The additional cut $\Delta\phi(j_3, \not{E}_T) > 0.4$ is only applied if a third jet with $p_T^{j_3} > 40\,\text{GeV}$ is present.

Applying these cuts at the level of a pure NLO simulation yields for the total cross sections for squark (anti)squark production combined with the subsequent decays in the two benchmark scenarios 10.3.6* and 10.4.5 the results given in the first row of Table 9. Matching these NLO results with a parton shower hardly affects the outcome after using the cuts defined in Eq. (37), as can be inferred from the results obtained with Pythia and the Herwig++ default shower listed in the second and third row, respectively. Note that due to the mixture of cuts on inclusive and exclusive quantities the rates predicted by the two showers are slightly larger compared to the NLO case. Moreover, the two parton showers yield identical rates within 1–2 %.

In order to compare these results obtained with our new calculations and implementations with the values determined according to the setup used so far for the simulation of these processes we proceed as follows: first the production and decays of the squarks are simulated with LO accuracy. The resulting events are reweighted with a common K-factor for squark–antisquark or squark pair production, which is obtained from Prospino, i.e. assuming degenerate squark masses and averaging over all channels. Each individual production channel is then multiplied with the corresponding NLO branching ratios for the produced squarks. The rescaled events are subsequently processed with the Pythia and the Herwig++ default shower, neglecting again effects of hadronization, MPI, etc. The results obtained with this approximate setup after applying the event selection cuts defined in Eq. (37) are summarized in the last two rows of Table 9. Comparing these total rates with those obtained in the full simulation one notes that the discrepancy is almost negligible in case of squark pair production, but amounts to 15–20 % for squark–antisquark production. This discrepancy is mainly caused by assuming a common K-factor for all subchannels instead of using the exact results with individual K-factors when combining production with decay. This effect in squark–antisquark production has already been demonstrated in Sect. 4.3.1 for the case of LO decays. In squark pair production, however, subchannels with K-factors close to the global K-factor have large branching ratios and therefore the exact and the approximate method give similar results. These examples illustrate that in order to obtain precise predictions it is not in all cases sufficient to use the approximate approach.

5 Conclusions

One of the main tasks of the LHC is the search for beyond the SM physics, in particular supersymmetry. At the high-energy run of the LHC coloured SUSY particles can be produced with masses up to the multi-TeV range. In order to find these particles and be able to measure their properties, reliable predictions for the production cross sections both at the inclusive and at the exclusive level are mandatory. In this paper we continue our effort in providing accurate theoretical predictions by presenting results for the squark–antisquark production of the first two generations at NLO SUSY-QCD without making any simplifying assumptions on the sparticle masses and by treating the different subchannels individually. As developed in our previous paper [54] we have performed the subtraction of possible on-shell intermediate gluinos in a gauge-invariant approach and compared to several methods

proposed in the literature. While in squark pair production for the investigated scenarios the differences in the total rates turned out to be negligible and quite small for distributions, in squark–antisquark production, where the contributions of the qg initiated channels are more important, larger differences were found. They amount to about 4 % for the inclusive NLO cross section in the investigated scenario. Even larger effects are found in the distributions, where the discrepancies between the investigated methods can be up to 30 % in the p_T distribution of the radiated parton. The invariant mass distribution of the squark–antisquark pair is not affected by the chosen method, however, and only reflects the discrepancy in the total cross section.

The K-factor for squark–antisquark production has been found to be sizeable and positive with $K \equiv \sigma_{\mathrm{NLO}}/\sigma_{\mathrm{LO}} \approx 1.4$ and the scale uncertainty is strongly reduced by taking into account the NLO corrections. The comparison of the results for individual K-factors for the subchannels contributing to squark–antisquark production and the K-factor obtained after summing the cross sections differ significantly, so that the use of a global K-factor in general does not lead to accurate predictions. Combining the NLO production cross section with LO decays of the (anti)squark into the lightest neutralino and (anti)quark leads to discrepancies of about 10 % between the exact result and the one assuming a common K-factor. The more the branching ratios of the squarks for the specific decay channel under consideration differ, the more important the consistent treatment of the individual corrections becomes.

In a next step we have combined our results for squark pair and for squark–antisquark production with the decays of the final state (anti)squarks into the lightest neutralino and (anti)quark at NLO SUSY-QCD at fully differential level. In this context we have discussed two methods for the combination of production and decay with NLO accuracy in the kinematics. One is based on a Taylor expansion respecting unitarity, but suffering from possibly negative contributions. The second approach, which does not expand the total decay width entering the branching ratios of the decays, avoids this problem, however violates unitarity. The results for these two approximations and for the case where no expansion in the strong coupling is performed at all, differ by at most 4 % for the total cross sections. In the jet distributions the discrepancies between the two approximations can be up to 15 %, whereas in the $\not{E}_T$ distribution they are purely given by the discrepancy in the total cross sections. In view of these small deviations, in particular for the inclusive quantities, we have adopted the unitarity preserving approach in the remaining numerical analysis.

The influence of the NLO corrections on the distributions has been investigated for several observables. While in the $\not{E}_T$ distribution the deviation of the differential K-factor and the total one is of $\mathcal{O}(5\,\%)$, the K-factor for the p_T distributions of the two hardest jets can vary in a range of ± 40 %, hence the assumption of a constant K-factor clearly is not valid here any more.

In order to obtain realistic predictions for exclusive observables we have matched the NLO cross sections with parton showers using the Powheg-Box framework. The implementation is publicly available and can be downloaded from [60].

The matched NLO results have been interfaced with the p_T ordered shower of Pythia6 as well as the default shower and the Dipole shower of Herwig++. To allow for a consistent comparison of the three showers, in Pythia the starting scale for the radiation off the decay products had to be modified. The largest differences in the three shower predictions is found in the pseudorapidity distribution of the third hardest jet. Thus Herwig++ predicts more jets in the central region, which is particularly pronounced for squark–antisquark production in the investigated scenario. The comparison of the showered result with a pure NLO simulation shows small differences for more inclusive quantities. In more exclusive distributions, in particular Herwig++ shows large deviations from the pure NLO result, as e.g. in the predictions for the third hardest jet. To decide if this is an effect of the missing truncated shower or a relict of the way the phase space is populated would require further investigations and is beyond the scope of this work.

Finally, we performed a cut-based analysis of the total cross sections in two benchmark scenarios using realistic event selection cuts taken from an ATLAS analysis. Comparing our results with the approximate approach used by the experiments revealed small discrepancies for squark pair production, but up to 20 % differences for squark–antisquark production. This effect could be traced back to assuming a common K-factor for the production cross sections of all subchannels instead of using the exact results. These examples show that the effects can be sizeable and precise theoretical predictions should take into account the full NLO calculation for the production processes, consistently combined with the squark decays at NLO.

The reliable exploitation and interpretation of the LHC data in the search for new physics requires accurate theoretical predictions for production and decay of SUSY particles including higher order corrections not only for inclusive quantities but also for distributions. Our results for the fully differential calculation of the SUSY-QCD corrections to squark pair and squark–antisquark production combined with their subsequent decay at NLO SUSY-QCD and matched with parton showers show that the independent treatment of the contributing subchannels is essential and that differential K-factors can not be assumed to be flat. The results presented here are the next step in our program of providing a fully differential description of SUSY particle production and decay at the LHC.

Acknowledgments M.P. thanks Laura Jenniches and Alexander Mück for useful discussions. C.H. has been supported by the 'Karlsruher Schule f++r Elementarteilchen- und Astroteilchenphysik: Wissenschaft und Technologie (KSETA)'. This work has been supported by the DFG SFB/TR9 "Computational Particle Physics". The research of M.S. is supported in part by the European Commission through the "HiggsTools" Initial Training Network PITN-GA-2012-316704. Last but not least, we thank Carlo Oleari for making our code publicly available via the Powheg-Box website.

References

1. D. Volkov, V. Akulov, Is the neutrino a goldstone particle? Phys. Lett. B **46**, 109–110 (1973)
2. Y. Golfand, E. Likhtman, Extension of the algebra of Poincare group generators and violation of p invariance. JETP Lett. **13**, 323–326 (1971)
3. P. Ramond, Dual theory for free fermions. Phys. Rev. D **3**, 2415–2418 (1971)
4. J. Wess, B. Zumino, Supergauge transformations in four-dimensions. Nucl. Phys. B **70**, 39–50 (1974)
5. J. Wess, B. Zumino, A Lagrangian model invariant under supergauge transformations. Phys. Lett. B **49**, 52 (1974)
6. M. Sohnius, Introducing supersymmetry. Phys. Rep. **128**, 39–204 (1985)
7. H.P. Nilles, Supersymmetry, supergravity and particle physics. Phys. Rep. **110**, 1–162 (1984)
8. H.E. Haber, G.L. Kane, The search for supersymmetry: probing physics beyond the standard model. Phys. Rep. **117**, 75–263 (1985)
9. J. Gunion, H.E. Haber, Higgs bosons in supersymmetric models. 1. Nucl. Phys. B **272**, 1 (1986)
10. J. Gunion, H.E. Haber, Higgs bosons in supersymmetric models. 2. Implications for phenomenology. Nucl. Phys. B **278**, 449 (1986)
11. J.F. Gunion, H.E. Haber, Higgs bosons in supersymmetric models. 3. Decays into neutralinos and charginos. Nucl. Phys. B **307**, 445 (1988)
12. CMS Collaboration, Projected performance of an upgraded CMS detector at the LHC and hl-LHC: contribution to the snowmass process. arXiv:1307.7135
13. ATLAS Collaboration, Physics at a high-luminosity LHC with ATLAS. arXiv:1307.7292 [hep-ex]
14. Y. Gershtein, M. Luty, M. Narain, L.T. Wang, D. Whiteson et al., Working group report: new particles, forces, and dimensions. arXiv:1311.0299 [hep-ex]
15. G.L. Kane, J. Leveille, Experimental constraints on gluino masses and supersymmetric theories. Phys. Lett. B **112**, 227 (1982)
16. P. Harrison, C. Llewellyn Smith, Hadroproduction of supersymmetric particles. Nucl. Phys. B **213**, 223 (1983)
17. E. Reya, D. Roy, Supersymmetric particle production at p anti-p collider energies. Phys. Rev. D **32**, 645 (1985)
18. S. Dawson, E. Eichten, C. Quigg, Search for supersymmetric particles in hadron–hadron collisions. Phys. Rev. D **31**, 1581 (1985)
19. W. Beenakker, R. Hopker, M. Spira, P. Zerwas, Squark production at the Tevatron. Phys. Rev. Lett. **74**, 2905–2908 (1995). arXiv:hep-ph/9412272
20. W. Beenakker, R. Hopker, M. Spira, P. Zerwas, Gluino pair production at the Tevatron. Z. Phys. C **69**, 63–166 (1995). arXiv:hep-ph/9505416
21. W. Beenakker, R. Hopker, M. Spira, P. Zerwas, Squark and gluino production at hadron colliders. Nucl. Phys. B **492**, 51–103 (1997). arXiv:hep-ph/9610490
22. W. Beenakker, M. Kramer, T. Plehn, M. Spira, P. Zerwas, Stop production at hadron colliders. Nucl. Phys. B **515**, 3–14 (1998). arXiv:hep-ph/9710451
23. U. Langenfeld, S.-O. Moch, Higher-order soft corrections to squark hadro-production. Phys. Lett. B **675**, 210–221 (2009). arXiv:0901.0802 [hep-ph]
24. A. Kulesza, L. Motyka, Threshold resummation for squark–antisquark and gluino-pair production at the LHC. Phys. Rev. Lett. **102**, 111802 (2009). arXiv:0807.2405 [hep-ph]
25. A. Kulesza, L. Motyka, Soft gluon resummation for the production of gluino–gluino and squark–antisquark pairs at the LHC. Phys. Rev. D **80**, 095004 (2009). arXiv:0905.4749 [hep-ph]
26. W. Beenakker, S. Brensing, M. Kramer, A. Kulesza, E. Laenen, I. Niessen, Soft-gluon resummation for squark and gluino hadroproduction. JHEP **0912**, 041 (2009). arXiv:0909.4418 [hep-ph]
27. W. Beenakker, S. Brensing, M. Kramer, A. Kulesza, E. Laenen, I. Niessen, Supersymmetric top and bottom squark production at hadron colliders. JHEP **1008**, 098 (2010). arXiv:1006.4771 [hep-ph]
28. W. Beenakker, S. Brensing, M. Kramer, A. Kulesza, E. Laenen, I. Niessen, NNLL resummation for squark–antisquark pair production at the LHC. JHEP **1201**, 076 (2012). arXiv:1110.2446 [hep-ph]
29. W. Beenakker, S. Brensing, M. Kramer, A. Kulesza, E. Laenen et al., Squark and gluino hadroproduction. Int. J. Mod. Phys. A **26**, 2637–2664 (2011). arXiv:1105.1110 [hep-ph]
30. C. Borschensky, M. Krämer, A. Kulesza, M. Mangano, S. Padhi et al., Squark and gluino production cross sections in pp collisions at $\sqrt{s}$ = 13, 14, 33 and 100 TeV. arXiv:1407.5066 [hep-ph]
31. M. Beneke, P. Falgari, C. Schwinn, Threshold resummation for pair production of coloured heavy (s)particles at hadron colliders. Nucl. Phys. B **842**, 414–474 (2011). arXiv:1007.5414 [hep-ph]
32. P. Falgari, C. Schwinn, C. Wever, NLL soft and Coulomb resummation for squark and gluino production at the LHC. JHEP **1206**, 052 (2012). arXiv:1202.2260 [hep-ph]
33. W. Beenakker, T. Janssen, S. Lepoeter, M. Kramer, A. Kulesza, E. Laenen, I. Niessen, S. Thewes, T. Van Daal, Towards NNLL resummation: hard matching coefficients for squark and gluino hadroproduction. arXiv:1304.6354 [hep-ph]
34. A. Broggio, A. Ferroglia, M. Neubert, L. Vernazza, L.L. Yang, Approximate NNLO predictions for the stop-pair production cross section at the LHC. arXiv:1304.2411 [hep-ph]
35. M.R. Kauth, A. Kress, J.H. Kuhn, Gluino–squark production at the LHC: the threshold. JHEP **1112**, 104 (2011). arXiv:1108.0542 [hep-ph]
36. M.R. Kauth, J.H. Kuhn, P. Marquard, M. Steinhauser, Gluino pair production at the LHC: the threshold. Nucl. Phys. B **857**, 28–64 (2012). arXiv:1108.0361 [hep-ph]
37. K. Hagiwara, H. Yokoya, Bound-state effects on gluino-pair production at hadron colliders. JHEP **0910**, 049 (2009). arXiv:0909.3204 [hep-ph]
38. S. Bornhauser, M. Drees, H.K. Dreiner, J.S. Kim, Electroweak contributions to squark pair production at the LHC. Phys. Rev. D **76**, 095020 (2007). arXiv:0709.2544 [hep-ph]
39. A. Arhrib, R. Benbrik, K. Cheung, T.-C. Yuan, Higgs boson enhancement effects on squark-pair production at the LHC. JHEP **1002**, 048 (2010). arXiv:0911.1820 [hep-ph]
40. W. Hollik, M. Kollar, M.K. Trenkel, Hadronic production of top-squark pairs with electroweak NLO contributions. JHEP **0802**, 018 (2008). arXiv:0712.0287 [hep-ph]

41. M. Beccaria, G. Macorini, L. Panizzi, F. Renard, C. Verzegnassi, Stop–antistop and sbottom–antisbottom production at LHC: a one-loop search for model parameters dependence. Int. J. Mod. Phys. A **23**, 4779–4810 (2008). arXiv:0804.1252 [hep-ph]
42. W. Hollik, E. Mirabella, Squark–anti-squark pair production at the LHC: the electroweak contribution. JHEP **0812**, 087 (2008). arXiv:0806.1433 [hep-ph]
43. W. Hollik, E. Mirabella, M.K. Trenkel, Electroweak contributions to squark–gluino production at the LHC. JHEP **0902**, 002 (2009). arXiv:0810.1044 [hep-ph]
44. E. Mirabella, NLO electroweak contributions to gluino pair production at hadron colliders. JHEP **0912**, 012 (2009). arXiv:0908.3318 [hep-ph]
45. J. Germer, W. Hollik, E. Mirabella, M.K. Trenkel, Hadronic production of squark–squark pairs: the electroweak contributions. JHEP **1008**, 023 (2010). arXiv:1004.2621 [hep-ph]
46. J. Germer, W. Hollik, E. Mirabella, Hadronic production of bottom-squark pairs with electroweak contributions. JHEP **1105**, 068 (2011). arXiv:1103.1258 [hep-ph]
47. W. Beenakker, R. Hopker, M. Spira, PROSPINO: a program for the production of supersymmetric particles in next-to-leading order QCD. arXiv:hep-ph/9611232
48. W. Hollik, J. M. Lindert, D. Pagani, NLO corrections to squark–squark production and decay at the LHC. arXiv:1207.1071 [hep-ph]
49. W. Hollik, J.M. Lindert, D. Pagani, On cascade decays of squarks at the LHC in NLO QCD. arXiv:1303.0186 [hep-ph]
50. J. Germer, W. Hollik, J.M. Lindert, E. Mirabella, Top-squark pair production at the LHC: a complete analysis at next-to-leading order. arXiv:1404.5572 [hep-ph]
51. R. Boughezal, M. Schulze, Precise predictions for top-quark plus missing-energy signatures at the LHC. Phys. Rev. Lett. **110**(19), 192002 (2013). arXiv:1212.0898 [hep-ph]
52. R. Boughezal, M. Schulze, $t\bar{t}$+large missing energy from top-quark partners: a comprehensive study at next-to-leading order QCD. Phys. Rev. D **88**(11), 114002 (2013). arXiv:1309.2316 [hep-ph]
53. D. Goncalves-Netto, D. Lopez-Val, K. Mawatari, T. Plehn, I. Wigmore, Automated squark and gluino production to next-to-leading order. arXiv:1211.0286 [hep-ph]
54. R. Gavin, C. Hangst, M. Krämer, M. M++hlleitner, M. Pellen, E. Popenda, M. Spira, Matching squark pair production at NLO with parton showers.JHEP **10**, 187 (2013). arXiv:1305.4061 [hep-ph]
55. E. Popenda, Higher order corrections to supersymmetric production and decay processes at the LHC. Phd thesis, Karlsruhe Institute of Technology (2012). (digbib.ubka.uni-karlsruhe.de:1000035939)
56. C. Hangst, Matching squark production and decay at next-to-leading order accuracy with parton showers. Phd thesis, Karlsruhe Institute of Technology (2014). (digbib.ubka.uni-karlsruhe.de:1000041155)
57. P. Nason, A new method for combining NLO QCD with shower Monte Carlo algorithms. JHEP **0411**, 040 (2004). arXiv:hep-ph/0409146
58. S. Frixione, P. Nason, C. Oleari, Matching NLO QCD computations with parton shower simulations: the POWHEG method. JHEP **0711**, 070 (2007). arXiv:0709.2092 [hep-ph]
59. S. Alioli, P. Nason, C. Oleari, E. Re, A general framework for implementing NLO calculations in shower Monte Carlo programs: the Powheg Box. JHEP **1006**, 043 (2010). arXiv:1002.2581 [hep-ph]
60. http://powhegbox.mib.infn.it/
61. J. Kublbeck, M. Bohm, A. Denner, Feynarts: computer algebraic generation of Feynman graphs and amplitudes. Comput. Phys. Commun. **60**, 165–180 (1990)
62. T. Hahn, Generating Feynman diagrams and amplitudes with FeynArts 3. Comput. Phys. Commun. **140**, 418–431 (2001). arXiv:hep-ph/0012260
63. T. Hahn, C. Schappacher, The implementation of the minimal supersymmetric standard model in FeynArts and FormCalc. Comput. Phys. Commun. **143**, 54–68 (2002). arXiv:hep-ph/0105349
64. T. Hahn, M. Perez-Victoria, Automatized one loop calculations in four-dimensions and D-dimensions. Comput. Phys. Commun. **118**, 153–165 (1999). arXiv:hep-ph/9807565
65. T. Hahn, A mathematica interface for FormCalc-generated code. Comput. Phys. Commun. **178**, 217–221 (2008). arXiv:hep-ph/0611273
66. G. van Oldenborgh, FF: a package to evaluate one loop Feynman diagrams. Comput. Phys. Commun. **66**, 1–15 (1991)
67. G. 't Hooft, M. Veltman, Regularization and renormalization of gauge fields. Nucl. Phys. B **44**, 189–213 (1972)
68. K.G. Wilson, The renormalization group and strong interactions. Phys. Rev. D **3**, 1818 (1971)
69. K.G. Wilson, M.E. Fisher, Critical exponents in 3.99 dimensions. Phys. Rev. Lett. **28**, 240–243 (1972)
70. C. Bollini, J. Giambiagi, Dimensional renormalization: the number of dimensions as a regularizing parameter. Nuovo Cim. B **12**, 20–25 (1972)
71. J. Ashmore, A method of gauge invariant regularization. Lett. Nuovo Cim. **4**, 289–290 (1972)
72. J.C. Collins, F. Wilczek, A. Zee, Low-energy manifestations of heavy particles: application to the neutral current. Phys. Rev. D **18**, 242 (1978)
73. W. Bernreuther, W. Wetzel, Decoupling of heavy quarks in the minimal subtraction scheme. Nucl. Phys. B **197**, 228 (1982)
74. R. Harlander, L. Mihaila, M. Steinhauser, Two-loop matching coefficients for the strong coupling in the MSSM. Phys. Rev. D **72**, 095009 (2005). arXiv:hep-ph/0509048
75. S.P. Martin, M.T. Vaughn, Regularization dependence of running couplings in softly broken supersymmetry. Phys. Lett. B **318**, 331–337 (1993). arXiv:hep-ph/9308222
76. R. Mertig, M. Böhm, A. Denner, Feyn Calc—computer-algebraic calculation of Feynman amplitudes. Comput. Phys. Commun. **64**, 345–359 (1991)
77. J. Alwall, M. Herquet, F. Maltoni, O. Mattelaer, T. Stelzer, MadGraph 5: going beyond. JHEP **1106**, 128 (2011). arXiv:1106.0522 [hep-ph]
78. H. Murayama, I. Watanabe, K. Hagiwara, HELAS: Helicity amplitude subroutines for Feynman diagram evaluations. KEK-91-11 (1992)
79. T. Kinoshita, Mass singularities of Feynman amplitudes. J. Math. Phys. **3**, 650–677 (1962)
80. T. Lee, M. Nauenberg, Degenerate systems and mass singularities. Phys. Rev. **133**, B1549–B1562 (1964)
81. S. Frixione, Z. Kunszt, A. Signer, Three jet cross-sections to next-to-leading order. Nucl. Phys. B **467**, 399–442 (1996). arXiv:hep-ph/9512328
82. A. Denner, S. Dittmaier, The complex-mass scheme for perturbative calculations with unstable particles. Nucl. Phys. Proc. Suppl. **160**, 22–26 (2006). arXiv:hep-ph/0605312
83. S. Frixione, E. Laenen, P. Motylinski, B.R. Webber, C.D. White, Single-top hadroproduction in association with a W boson. JHEP **0807**, 029 (2008). arXiv:0805.3067 [hep-ph]
84. S. AbdusSalam, B. Allanach, H. Dreiner, J. Ellis, U. Ellwanger et al., Benchmarkmodels, planes, lines and points for future SUSY searches at the LHC. Eur. Phys. J. C **71**, 1835 (2011). arXiv:1109.3859 [hep-ph]
85. R. Frederix, S. Frixione, F. Maltoni, T. Stelzer, Automation of next-to-leading order computations in QCD: the FKS subtraction. JHEP **0910**, 003 (2009). arXiv:0908.4272 [hep-ph]

86. A. Djouadi, W. Hollik, C. Junger, QCD corrections to scalar quark decays. Phys. Rev. D **55**, 975–6985 (1997). arXiv:hep-ph/9609419
87. J.M. Campbell, R.K. Ellis, F. Tramontano, Single top production and decay at next-to-leading order. Phys. Rev. D **70**, 094012 (2004). arXiv:hep-ph/0408158
88. T. Huber, D. Maitre, HypExp: a mathematica package for expanding hypergeometric functions around integer-valued parameters. Comput. Phys. Commun. **175**, 122–144 (2006). arXiv:hep-ph/0507094
89. T. Huber, D. Maitre, HypExp 2, expanding hypergeometric functions about half-integer parameters. Comput. Phys. Commun. **178**, 755–776 (2008). arXiv:0708.2443 [hep-ph]
90. L. Jenniches, Finite width effects in supersymmetric cascade decays.Master thesis, RWTH University, Aachen, Germany (2011)
91. M. Muhlleitner, A. Djouadi, Y. Mambrini, SDECAY: a Fortran code for the decays of the supersymmetric particles in the MSSM. Comput. Phys. Commun. **168**, 46–70 (2005). arXiv:hep-ph/0311167
92. Particle Data Group Collaboration, J. Beringer et al., Review of particle physics (RPP). Phys. Rev. D **86**, 010001 (2012)
93. W. Beenakker, R. Hopker, P. Zerwas, SUSY QCD decays of squarks and gluinos. Phys. Lett. B **378**, 159–166 (1996). arXiv:hep-ph/9602378
94. W. Beenakker, R. Hopker, T. Plehn, P. Zerwas, Stop decays in SUSY QCD. Z. Phys. C **75**, 349–356 (1997). arXiv:hep-ph/9610313
95. V.S. Fadin, V.A. Khoze, A.D. Martin, How suppressed are the radiative interference effects in heavy instable particle production? Phys. Lett. B **320**, 141–144 (1994). arXiv:hep-ph/9309234
96. V.S. Fadin, V.A. Khoze, A.D. Martin, Interference radiative phenomena in the production of heavy unstable particles. Phys. Rev. D **49**, 2247–2256 (1994)
97. K. Melnikov, M. Schulze, NLO QCD corrections to top quark pair production and decay at hadron colliders. JHEP **0908**, 049 (2009). arXiv:0907.3090 [hep-ph]
98. P. Richardson, A. Wilcock, Monte Carlo Simulation of hard radiation in decays in beyond the standard model physics in Herwig++. Eur. Phys. J. C **74**, 2713 (2014). arXiv:1303.4563 [hep-ph]
99. ATLAS Collaboration Collaboration, Search for squarks and gluinos with the ATLAS detector in final states with jets and missing transverse momentum and 20.3 fb^{-1} of $\sqrt{s} = 8$ TeV proton–proton collision data. ATLAS-CONF-2013-047
100. CMS Collaboration Collaboration, S. Chatrchyan et al., Search for new physics in the multijet and missing transverse momentum final state in proton-proton collisions at $\sqrt{s} = 8$ TeV. arXiv:1402.4770 [hep-ex]
101. B. Allanach, SOFTSUSY: a program for calculating supersymmetric spectra. Comput. Phys. Commun. **143**, 305–331 (2002). arXiv:hep-ph/0104145
102. M. Whalley, D. Bourilkov, R. Group, The Les Houches accord PDFs (LHAPDF) and LHAGLUE. arXiv:hep-ph/0508110
103. J. Pumplin, D. Stump, J. Huston, H. Lai, P.M. Nadolsky et al., New generation of parton distributions with uncertainties from global QCD analysis. JHEP **0207**, 012 (2002). arXiv:hep-ph/0201195
104. H.-L. Lai, M. Guzzi, J. Huston, Z. Li, P.M. Nadolsky et al., New parton distributions for collider physics. Phys. Rev. D **82**, 074024 (2010). arXiv:1007.2241 [hep-ph]
105. M. Cacciari, G.P. Salam, Dispelling the N^3 myth for the k_t jet-finder. Phys. Lett. B **641**, 57–61 (2006). arXiv:hep-ph/0512210
106. M. Cacciari, G.P. Salam, G. Soyez, FastJet user manual. Eur. Phys. J. C **72**, 1896 (2012). arXiv:1111.6097 [hep-ph]
107. M. Cacciari, G.P. Salam, G. Soyez, The anti-k(t) jet clustering algorithm. JHEP **0804**, 063 (2008). arXiv:0802.1189 [hep-ph]
108. T. Sjostrand, S. Mrenna, P.Z. Skands, PYTHIA 6.4 physics and manual. JHEP **0605**, 026 (2006). arXiv:hep-ph/0603175
109. P.Z. Skands, Tuning Monte Carlo generators: the Perugia tunes. Phys. Rev. D **82**, 074018 (2010). arXiv:1005.3457 [hep-ph]
110. M. Bahr, S. Gieseke, M. Gigg, D. Grellscheid, K. Hamilton et al., Herwig++ physics and manual. Eur. Phys. J. C **C58**, 639–707 (2008). arXiv:0803.0883 [hep-ph]
111. S. Platzer, S. Gieseke, Coherent parton showers with local recoils. JHEP **1101**, 024 (2011). arXiv:0909.5593 [hep-ph]
112. S. Platzer, S. Gieseke, Dipole showers and automated NLO matching in Herwig++. Eur. Phys. J. C **72**, 2187 (2012). arXiv:1109.6256 [hep-ph]
113. K. Arnold, L. d'Errico, S. Gieseke, D. Grellscheid, K. Hamilton et al., Herwig++ 2.6 release note. arXiv:1205.4902 [hep-ph]